POLY(ADP-RIBOSE) POLYMERASE-1 INHIBITION POTENTIATES CELL DEATH AND PHOSPHORYLATION OF DNA DAMAGE RESPONSE PROTEINS IN OXIDATIVE STRESSED RETINAL CELLS

Sandra M. Martín-Guerrero[a], Pedro Casado[b], José A. Muñoz-Gámez[c], María-Carmen Carrasco[a], Julio Navascués[a], Miguel A. Cuadros[a], Juan F. López-Giménez[d], Pedro R. Cutillas[b], David Martín-Oliva[a]

[a]Departamento de Biología Celular. Facultad de Ciencias. Universidad de Granada. Spain
[b]Cell Signalling and proteomics Group. Centre of Haemato-Oncology. Barts Cancer Institute. Queen Mary University of London. United Kingdom
[c]Hospital Universitario San Cecilio de Granada. FIBAO. Spain
[d]Instituto de Parasitología y Biomedicina López-Neyra (Granada). CSIC. Spain

Corresponding author:

David Martín-Oliva. Departamento de Biología Celular. Facultad de Ciencias. . Universidad de Granada. E-18071 Granada. Spain

e-mail: dmoliva@ugr.es

ABSTRACT

Oxidative stress (OxS) is involved in the development of cell injures occurring in retinal diseases while Poly(ADP-ribose) Polymerase-1 (PARP-1) is a key protein involved in the repair of the DNA damage caused by OxS. Inhibition of PARP-1 activity with the pharmacological inhibitor PJ34 in mouse retinal explants subjected to H_2O_2-induced oxidative damage resulted in an increase of apoptotic cells. Reduction of cell growth was also observed in the mouse cone like cell line 661W in the presence of PJ34 under OxS conditions. Mass spectrometry-based phosphoproteomics analysis performed in 661W cells determined that OxS induced significant changes in the phosphorylation in 1807 of the 8131 peptides initially detected. Blockade of PARP-1 activity after the oxidative treatment additionally increased the phosphorylation of multiple proteins, many of them at SQ motifs and related to the DNA-damage response (DDR). These motifs are substrates of the kinases ATM/ATR, which play a central role in DDR. Western blot analysis confirmed that the ATM/ATR activity measured and the phosphorylation at SQ motifs of ATM/ATR substrates was augmented when PARP-1 activity was inhibited under OxS conditions, in 661W cells. Phosphorylation of ATM/ATR substrates, including the phosphorylation of the histone H2AX were also induced in organotypic cultures of retinal explants subjected to PARP-1 inhibition during exposure to OxS. In conclusion, inhibition of PARP-1 increased the phosphorylation and hence the activation of several proteins involved in the response to DNA damage, like the ATM protein kinase. This finally resulted in an augmented injury in mouse retinal cells suffering from OxS. Therefore, the inhibition of PARP-1 activity may have a negative outcome in the treatment of retinal diseases in which OxS is involved.

Keywords: Photoreceptor; oxidative stress; phosphoproteomic; Poly(ADP-ribose) Polymerase-1; DNA damage; cell death.

Abbreviations: ATM, Ataxia-Teleangiectasia Mutated; ATR, ATM and Rad-3 Related; BRCA1, Breast cancer type 1 susceptibility protein; DDR, DNA-damage response; DSBs, double-strand breaks; GCL, ganglion cell layer; INL, inner nuclear layer; LC-MS/MS, Liquid chromatography tandem-mass spectrometry; MDC1, Mediator of DNA damage checkpoint protein 1; ONL, outer nuclear layer; OxS, Oxidative stress; PARP-1, Poly(ADP-ribose) Polymerase-1; PAR, Poly(ADP-Ribose); ROS, Reactive oxygen species; SDS-PAGE, sodium dodecyl sulphate-polyacrylamide gel electrophoresis; SSBs, single-strand breaks; TUNEL, terminal deoxynucleotidyl transferase dUTP nick end labeling.

1. Introduction

Physiological levels of reactive oxygen species (ROS), produced mainly by the normal respiration of mitochondria, are eliminated by the antioxidant systems of the cells. However, when the production of ROS highly increases, as after an oxidative insult, this increase cannot be correctly counteracted by the antioxidant systems, and the cells suffer an oxidative stress (OxS). Although the antioxidant systems normally eliminate the elevated ROS levels generated as a consequence of the high oxygen consumption caused by excitatory signals in retinal cells, a further increase of ROS is in the center of several retinal pathologies. In fact, ROS can cause harm to cell components and trigger cell death (Nishimura et al., 2017; Schieber and Chandel, 2014). Among other effects, ROS induce harms to the DNA that cells try to solve by triggering the DNA-damage response (DDR) (Jackson and Bartek, 2009; Polo and Jackson, 2011). DDR activates a protein kinase cascade that results in the phosphorylation of hundreds of proteins involved in different aspects of genomic stability, as DNA replication, DNA repair, control of cell cycle and cell death. The kinases ATM (Ataxia-Teleangiectasia Mutated) and ATR (ATM and Rad-3 Related) are main components of this phosphorylation cascade, acting at the beginning of this pathway. Activated ATM and ATR phosphorylate their substrates mainly on serine (Ser, S) and threonine (Thr, T) residues preceding a glutamine (Gln, Q) residue. Therefore, proteins with regions containing high density of Ser/Thr + Gln residues (termed SQ/TQ motifs) are likely phosphorylated by ATM and ATR (Kastan and Lim, 2000; Traven and Heierhorst, 2005).

Poly(ADP-Ribose) Polymerase-1 (PARP-1) is a component of the DDR and the founding member of the PARP family. PARP-1 regulates the repair of DNA by catalyzing the polymerization of ADP-ribose units (PAR polymer) on target proteins,

including itself (D'Amours et al., 1999; Schreiber et al., 2006); although other members of the PARP family catalyze similar processes, about 90% of the formation of PAR polymer is due to the activity of PARP-1 (Shieh et al., 1998).

PARP-1 participates in the sensing and/or repair of DNA breaks in most eukaryote cells (Dantzer et al., 2000; Fisher et al., 2007). In line with that, PARP-1 defective cells show hypersensitivity to DNA damage and genomic instability (Caldecott, 2014). Defects in DNA single-strand breaks (SSBs) repair pathway, in which PARP-1 participate, have been associated with hereditary neurodegenerative diseases (Caldecott, 2008; Rass et al., 2007). However, over-activation of PARP-1 can greatly increase the consumption of NAD^+, thus diminishing the generation of ATP resulting in an energy failure that may eventually produce the death of the cell (Ha and Snyder, 1999). So, the activity of PARP-1 may have both beneficial and harmful effects for the survival of cells.

In this study, we analyze the response of mouse retinal cells to OxS caused by exposure to the pro-oxidant agent H_2O_2 when PARP-1 activity is present and when PARP-1 activity is pharmacologically blocked. For this analysis, we used two experimental models, organotypic cultures of retinal explants and 661W cells (an immortalized cell line that shows characteristics of photoreceptor cone cells). We found that the blockage of PARP-1 under OxS conditions in both models increased the phosphorylation at SQ motifs of proteins involved in the DDR pathway, decreased cell viability and increased injury.

2. Materials and methods

2.1. Obtaining, culture and treatment of retinal explants

Retinal explants were obtained from 12 days old (P12) postnatal C57BL/6 mice provided by the Animal Experimentation Service of the University of Granada (Spain). Experimental procedures were approved by the Animal Experimentation Ethics Committee of the University of Granada (permit number 26/04/2018/058) following the guidelines of the European Union Directive 2010/63/EU on the protection of animals used for scientific purposes.

The explants were prepared as indicated in Ferrer-Martin et al. (2014). In brief, P12 mice were killed by decapitation and enucleated; the isolated eyes were placed in Petri dishes containing Gey's balanced salt solution (Sigma, St. Louis, USA) supplemented with 5 mg/ml glucose (Sigma) and 50 IU-µg/ml penicillin-streptomycin (Invitrogen, Paisley, UK). The retina was isolated by removing the remaining ocular tissues and explants containing the central part of the retina were placed on membrane culture inserts (Millicell; Millipore, Bedford, MA) with vitreal side downward and cultured for a maximum of two days as described (Ferrer-Martin et al., 2014). In order to induce an oxidative damage, the explants were treated during 30 min with 3.5 mM of H_2O_2. Previously P12 explants were pre-incubated for 23.5 h in fresh medium composed of 50% Basal Medium Eagle with Earle's salts, 25% Hank's balanced salt solution and 25% horse serum, supplemented with 1 mM L-glutamine, 10 IU-µg/ml penicillin-streptomycin (all of Invitrogen) and 5 mg/ml glucose (Sigma). After the oxidative treatment, the explants were post-incubated in fresh medium for additional 12 or 24 h. Untreated explants were used as control.

The working solution of H_2O_2 was prepared from a commercial 30% solution of Hydrogen Peroxide (Sigma) kept at 4ºC in the dark. This solution was first diluted in

fresh medium to get an intermediate concentration of 0.1 M, which was additionally diluted in new fresh medium to reach the final concentration of H_2O_2; dilutions were prepared immediately before use.

PARP-1 activity was inhibited by the addition of 1 µM of PJ34 (cat # S7300, Selleckchem, USA) to the culture medium. PJ34 is a water-soluble and cell-permeable phenanthridinone derivative which selectively inhibits the catalytic activity of PARP-1 and PARP-2 (EC_{50} = 20 nM) (Pellicciari et al., 2008). In order to obtain the complete PARP-1 inhibition PJ34 was administrated during pre-incubation time (16 h), during the oxidative treatment (30 min) and during the post-incubation time (12 or 24 h) after it. An overview of the different experimental treatments is shown in Fig. 1.

2.2. Culture and treatments of 661W cells

The mouse cell line 661W, a kind gift from Dr. Muayyad Al-Ubaidi (University of Oklahoma Health Sciences Center, Oklahoma City, OK), shows characteristics of photoreceptor cone cells (Tan et al., 2004). 661W cells were maintained as an adherent monolayer in Dulbecco's modification of Eagle medium (Sigma) supplemented with 10% fetal bovine serum (Sigma), L-glutamine solution (4 mM; Sigma) and antibiotics (100 µg/ml of streptomycin and 100 U/ml of penicillin), and incubated at 37 ºC in an atmosphere containing 5% CO_2. Oxidative damage was induced incubating the cells during 30 min in medium containing 1 mM H_2O_2 (working concentrations of H_2O_2 were prepared as described above); afterwards the cells were incubated in fresh medium, without H_2O_2, for different time depending of the experimental proceedings. PARP-1 activity was inhibited by the addition of 1 µM of PJ34 to the culture medium as we previously described (Martin-Guerrero et al., 2017);

thus, incubation with PJ34 began 16 h before the oxidative insult (pre-incubation time), was maintained during it, and continued after the insult (see Fig. 1).

2.3. Semithin sections of retinal explants

Retinal explants, incubated or not with PJ34, were fixed 24 h after the H_2O_2 treatment in a mixture of 2% glutaraldehyde in 0.05 M cacodylate buffer (pH 7.4) supplemented with 2 mM Cl_2Mg and 0.03 g/L sucrose for 2 h. Afterwards they were post-fixed in 1% osmium tetroxide for 1 h, dehydrated in graded series of ethanol, and embedded in epoxy resin. Semithin sections (0.5 µm thick) were stained with toluidine blue and examined under an Axiophot microscope (Zeiss, Oberkochen, Germany) with a 40X objective (original magnification x 400).

2.4 Immunohistochemical staining of γ-H2AX in retinal explants

Retinal explants, incubated or not with PJ34, were fixed for immunohistochemistry in a solution of paraformaldehyde-lysine-periodate (Yamato et al., 1984) 24 h after the oxidative treatment. The fixed explants were cryoprotected with 20% sucrose in PBS-0.1% Triton X-100 (PBS-Tr) and placed in 10% gelatin and 10% sucrose in PBS that was afterwards frozen in isopentane (-80 ºC). Twenty µm-thick cryosections attached to Superfrost slides (Menzel-Glasser, Braunschweig, Germany) were permeabilized in 0.2% PBS-Tr, washed in PBS with 0.1% Tween-20 (PBS-Tw) and blocked with 10% of normal goat serum in PBS (10% NGS; Sigma). Then, cryosections were incubated first overnight at 4ºC with anti-γ-H2AX antibody (cat # NB100-79967, Novus Biologicals, Cambridge, UK), diluted 1:200 in 5% NGS in PBS-Tw, and later with the secondary antibody Alexa fluor 488-conjugated goat anti-rabbit IgG (Molecular Probes, Eugene, OR) diluted 1:800 in 5% NGS in PBS-Tw. Finally, nuclei were counterstained with 1

µg/ml DAPI (Sigma) and mounted with Fluor Save Reagent (cat # 345789; Calbiochem, Eugene, OR). As negative controls, the primary antibody was omitted in some slides. Confocal images were obtained with a Leica TCS-SP5 microscope (Leica, Wetzlar, Germany), stored in TIFF format and digitally prepared in Adobe Photoshop (Adobe Systems, San José, CA) by automatically adjusting their brightness and contrast. For quantitative studies, γ-H2AX-positive cells in the photoreceptors layer of three randomized fields per section were counted in three sections of three independent experiments by a Zeiss Axiophot fluorescent microscope using a 63X objective.

2.5. TUNEL assay and active caspase-3 detection in retinal explants

Cryosections from retinal explants were permeabilized in 0.2% PBS-Tr, washed in PBS and subjected to TUNEL (terminal deoxynucleotidyl transferase dUTP nick end labeling) assay. TUNEL assay is an established method to detect DNA fragmentation occuring in different kinds of cell death (Grasl-Kraupp et al., 1995). Retinal sections were incubated with 10 U/ml of terminal deoxynucleotididyl transferese (TdT) enzyme (cat # M1875; Promega, Madison, WI) in TdT buffer containing 0.2 nmol/ml of biotin-16-dUTP (Roche Diagnostics, Mannheim, Germany) for 1 h at 37ºC. In order to reveal the biotin labeling, sections were first washed in PBS and then incubated for 1 h at room temperature with Streptavidin Alexa Fluor 488 conjugate (Invitrogen) diluted 1:800 in PBS. Finally, the sections were washed and stained with 1 µg/ml DAPI.

Some sections were double-labeled with TUNEL and anti-active caspase-3 immunofluorescence. After performing the TUNEL staining, these sections were incubated overnight at 4ºC with anti-Active-Caspase-3 antibody (cat # AF835, R&D Systems, Minneapolis), diluted 1:50 in 5% NGS in PBS-Tw, and further with the

secondary antibody Alexa fluor 594-conjugated goat anti-rabbit IgG (diluted 1:800 in 5% NGS in PBS-Tw). Nuclei were counterstained with DAPI and mounted with Fluor Save Reagent. As negative controls, TdT reaction and primary antibody were omitted in some slides. TUNEL and/or active caspase-3 positive cells in all layers of the retina were recorded by the Leica TCS-SP5 Confocal Microscope. TUNEL positive cells in the photoreceptors layer of three randomized fields (at 630x magnification) per section were counted in three cryosections of three independent experiments similarly to that previously described by Doonan et al. (2009).

2.6. Annexin V and propidium iodide apoptosis assay

Apoptotic cell death was measured by flow cytometry using an Annexin V/propidium iodide assay in retinal explants 24 h after the oxidative treatment in absence or presence of PJ34 as above described. In this case, retinal explants were detached from the membrane insert and dissociated at 4 ºC using a Dounce homogenizer (Pobel, Madrid, Spain). The resulting suspension was passed several times through an insulin syringe with a 29-gauge needle (diameter 0.33 mm). Then, cells were incubated with 10 µg/ml of propidium iodide solution (Sigma) and 10 µl of APC Annexin V (cat # 550474, BD Biosciences, Erembodegem, Belgium) in 1 ml of cold 1x Annexin V Binding Buffer (Immunostep, Salamanca, Spain) for 15 min at room temperature in darkness. Samples were analyzed by flow cytometry using the BD FACSAria III cytometer and the BD FACSDiva 8.0 software (BD Biosciences).

2.7. Western blotting

Protein extracts from retinal explants and 661W cells exposed to H_2O_2, in presence or absence of PJ34, were obtained in RIPA buffer containing 1 mM of the phosphatase

inhibitor NaF (Sigma) and a protease inhibitor cocktail (F. Hoffmann-La Roche Ltd, Switzerland). After quantification by Bradford, proteins were separated in SDS-PAGE and transferred onto PVDF membranes (Bio-Rad, Hercules, CA). Blots were blocked and incubated with primary antibody solution and then with the corresponding peroxidase-conjugated secondary antibody solution. The antibody reaction was documented with the ChemiDoc-It Imaging System (UVP, Cambridge, UK) using a chemiluminescence reagent and densitometric analyses were carried out with ImageJ software (Schneider et al., 2012). The primary antibodies used were: anti-Phospho-ATM/ATR Substrate Motif [pSQ] antibody (1:1000 dilution; Cat # 9607S, Cell Signaling Technology, Leiden, Netherlands); anti-PAR antibody (1:1000 dilution; cat # 4335-MC-100, Trevigen, Gaithersburg, MD) that recognizes the product of PARP-1, Poly-ADP-ribose (PAR) polymers attached to target proteins; anti-β-actin (1:1000 dilution; cat # 170-5060, Sigma); and anti-β-tubulin (1:5000 dilution; cat # T2200, Sigma).

2.8. Mass spectrometry-based phosphoprotemics and Gene Ontology analysis on 661W cells

Phosproteomics studies were performed using liquid chromatography-tandem mass spectrometry (LC-MS/MS). 661W cells (in presence or absence of PJ34) were treated for 30 min with H_2O_2 and further incubated in fresh medium, with or without PJ34, for 6 h, and processed for phosphoproteomics analysis as already described (Casado et al., 2018; Wilkes and Cutillas, 2017). Peptide pellets, previously phosphoenriched with TiO_2, were resuspended in reconstitution buffer (20 fmol/µl enolase in 3% acetonitrile, 0.1% trifluoroacetic acid) and 5 µl of the solution were injected in an LC-MS/MS platform consisting in a Dionex UltiMate 3000 RSLC directly coupled to an Orbitrap Q-Exactive Plus mass spectrometer via an Easy Spray Source (Thermo Fisher

Scientific). Two technical replicates were performed for each biological sample in four independent experiments (n = 4).

Mascot Daemon (Perkins et al., 1999) was used to automate the identification of phosphopeptides from MS/MS spectra and Pescal (Cutillas and Vanhaesebroeck, 2007) to quantify the intensity values of the phosphopeptides. Peak areas from extracted ion chromatograms were used to calculate the intensity values of phosphopeptides (Cutillas and Vanhaesebroeck, 2007). Values of two technical replicates per sample were averaged, and intensity values for each phosphopeptide were normalized to total sample intensity.

Two tailed unpaired Students t-test and one-way analysis of variance (ANOVA) with Tukey's multiple comparison tests were used to determine significant differences in peptide phosphorylation between control and oxidative treatment with H_2O_2 (referred as "H_2O_2 treatment") and between control and oxidative treatment in presence of PJ34 (referred as "H_2O_2 + PJ34 treatment"). In order to measure the magnitude of the changes in protein phosphorylation induced by the treatments, a ratio of normalized intensity signals of phosphopeptides from treated cells divided by those of the respective untreated control samples was calculated and expressed as Log_2 of Ratio, and named as Fold Change (FC), as we show below:

$$FC = \log_2 \left(\frac{\text{average normalized signal intensity treated cells; n=4}}{\text{average normalized signal intensity untreated cells; n=4}} \right)$$

Phosphopeptides showing significant differences ($P < 0.05$) and FC ≥ 1 (up-regulated phosphopeptides) in H_2O_2 and in H_2O_2 + PJ34 treatments were selected for Gene Ontology (GO) analysis using bioinformatics tools such as ClueGO (Bindea et al., 2009; Shannon et al., 2003) and DAVID (Huang da et al., 2009). A graphic representation (amino acid sequence logo) for the phosphorylated motifs present in

up-regulated phosphopeptides was generated using the Frequency Change Algorithm available in PhosphoSitePlus (http://www.phosphosite.org) (Hornbeck et al., 2015).

Additional experimental details on mass spectrometry-based phosphoprotemics and GO analysis are described in the Supplementary Materials and Methods (Appendix A).

2.9. Anti-PAR immunofluorescence on 661W cells

Cells exposed to H_2O_2 for 15 min in the presence or absence of PJ34 were fixed with ice-cold methanol-acetone (1:1) and incubated with the primary mouse monoclonal anti-PAR antibody (dilution 1:400; cat # ALX-804-220-R100, Enzo Life Sciences, Farmingdale, NY), and then with the secondary antibody Alexa fluor 488-conjugated goat anti-mouse IgG (Molecular Probes). Cell nuclei were counterstained with Hoechst 33342 (Sigma). The slides were analyzed using an Axiophot microscope (Zeiss, Oberkochen, Germany).

2.10. Cell cycle analysis and cell density determination in 661W cells

For cell cycle analysis, 661W cells cultured for 24 h after oxidative treatment (in presence or absence of PJ34) were detached from cell plates, fixed and stained with a propidium iodide solution (cat # PI/RNase, ImmunoStep). The percentage of cells at different phases of the cell cycle was determined by flow cytometry in a BD FACSAria II cytometer using the FACSDiva 8.0 software (BD Biosciences).

The sulforhodamine B (SRB) assay, based on the measurement of cellular protein content, was used for the determination of cell density. For this, cells were seeded on culture plates, incubated with H_2O_2 as described in previous sections and left to recover 0, 24, 48 and 72 h with or without PJ34 inhibitor. At each time point, cells were fixed in an ice-cold solution of 10% tri-chloro acetic acid (Sigma). Afterwards, plates

were washed, dried and stained with a SRB solution. Finally, optic density (OD) was measured at 492 nm in a microplate spectrophotometer reader (Multiskan Ascent, Thermo Scientific, Rockford, lL).

2.11. Statistical analysis

Data were expressed as mean ± SEM from at least three independent experiments. Unless otherwise specified, significant differences were determined using unpaired (for 661W cells) and paired (for retinal explants) two tail Student's t-test. One-way analysis of variance (ANOVA) with Tukey's multiple comparison tests was used to determine significance in flow citometry study for cell death determination and two-tail Mann-Witney test was used to assess significance in cell cycle analysis. The statistical analyses were performed using IBM-SPSS Statistics software (version 19.0; IBM Corp., Armonk, NY). A value of $P < 0.05$ was considered statistically significant.

3. Results

3.1. Changes in retinal explants after oxidative insult

Organotypic culture of retinal explants obtained from P12 mice were performed as indicated in Fig. 1. As previously described (Ferrer-Martin et al., 2014), untreated explants (control) showed a comparable cytoarchitecture to those of *in vivo* retinas of similar ages (Fig. 2A, left panel). However, retinal explants subjected to an oxidative treatment with 3.5 mM of H_2O_2, showed important changes in the cytoarchitecture: the outer (ONL) and the inner (INL) nuclear layers, and the ganglion cell (GCL) layers showed obvious signs of cellular degeneration and pyknosis (Fig. 2A, middle panel). Similar alterations were observed in explants suffering the oxidative insult in presence of the PARP-1 inhibitor PJ34 (Fig. 2A, right panel). It is worth to note that PJ34 had no noticeable effect on the explants in the absence of the oxidative insult (Supplementary Fig. 1 in Appendix B).

The amount of cell death in the different experimental conditions was determined by Annexin V/propidium iodide method and TUNEL assay. Firstly, Annexin V/propidium iodide method revealed a significant increase of Annexin V-positive and propidium iodide-negative cells (indicative of early apoptosis) in oxidative stressed retinal explants when PARP-1 activity was inhibited (see Supplementary Fig. 2 in Appendix B). Secondly, counts of the number of TUNEL-positive cells showed that cell death was statistically increased in the photoreceptor layer of retinal explants treated with H_2O_2 + PJ34 compared to those treated solely with H_2O_2 (Fig. 2B and C). Since DNA fragmentation detected by TUNEL assay has been related to different kinds of cell death, and so, its staining could not be considered a specific marker of apoptosis (Grasl-Kraupp et al., 1995), some TUNEL sections of retinal explants were further immunolabeled with anti-active caspase-3 antibody, a reliable marker of apoptotic cell

death (Duan et al., 2003). As we shown in Fig. 2B, most TUNEL-positive nuclei colocalized with active caspase-3 immunolabeling suggesting that H_2O_2 induces apoptotic cell death after oxidative treatment and PARP-1 inhibition by PJ34 inhibitor potentiates the apoptosis in the photoreceptor layer of retinal explants after oxidative treatment.

H_2O_2 induces cell death by promoting DNA breaks (Iloki-Assanga et al., 2015), and as PARP-1 is involved in DNA repair pathways, we next evaluated if the DNA damage induced by H_2O_2 treatment increased when PARP-1 is inhibited. For this, we detected by immunohistochemistry the presence of a phosphorylated form of the histone H2AX (γ-H2AX) in the retinal explants incubated in different conditions. γ-H2AX is involved in the recruitment of DDR proteins to regions of damaged DNA (Podhorecka et al., 2010), and it is therefore a marker of the presence of DNA breaks. γ-H2AX positive cells, predominantly localized in the INL and ONL, were more frequent in retinal explants subjected to oxidative insult respect to untreated retinal explants (Fig. 3A). Because TUNEL-positive cells statistically increased in the ONL when PARP-1 activity was inhibited by PJ34 compared to H_2O_2-treated retinal explants without PJ34 inhibitor, and cell death may be induced by DNA damage, we quantified the levels of γ-H2AX staining in this layer. We found a statistically increase in γ-H2AX staining (Fig. 3B) in presence of PJ34 inhibitor in the photoreceptor layer when compared to H_2O_2-treated retinal explants without PJ34 inhibitor.

Finally, we confirmed that the treatment with H_2O_2 induced in the retinal explants an increase in PARP-1 activity (measured by the formation of the PAR polymer, product of the activity of PARP-1) and that PJ34 inhibited the increase in PARP-1 activity induced by H_2O_2 (Fig. 3C).

In summary, inhibition of PARP-1 activity with PJ34 increases the retinal injury, the amount of cell death and the DNA damage of photoreceptor cells after an oxidative damage caused by the addition of H_2O_2.

3.2. Global changes in photoreceptor phosphoprotein expression after oxidative insult in 661W cells

As inhibition of PARP-1 activity increased the retinal injury in ONL after an oxidative insult, we investigated then if this insult induced modifications in the phosphoproteome of photoreceptor cells and whether these modifications affected the DNA damage/repair signaling. For that, we used the 661W cells as an *in vitro* model of photoreceptor cells (Tan et al., 2004). Initially, we established that the OxS induced an increment of the activity of PARP-1 activity (Fig 4A) and that PJ34 inhibitor blocked PAR synthesis in 661W cells treated with H_2O_2 (Fig. 4B and C). Most PAR polymer formation took place 15 min after the beginning of H_2O_2 treatment suggesting that PARP-1 activation is an early event after an oxidative damage in 661W cells (Fig. 4A).

Then, we investigated the effect of PARP-1 inhibition during oxidative stress on the phosphoproteome of 661W cells. The phosphoproteomic analysis was performed 6 h after the oxidative insult in order to assure that the proteins implicated in the affected pathways have been modified. Globally, we detected 8131 phosphopeptides, of which 1807 and 1874 showed significant changes ($P < 0.05$) in their expression in H_2O_2 and in H_2O_2 + PJ34 treatments (both compared to untreated cells), respectively. Volcano plots of all detected phosphopeptides show that H_2O_2 treatment significantly increased the phosphorylation of 524 peptides while 621 were increased in H_2O_2 + PJ34 treatment (Fig. 5A).

Therefore, the oxidative insult modifies the phosphorylation pattern of 661W cells and PARP-1 inhibition with PJ34 results in a further modification of this phosphoproteome signature.

3.3. Biological processes affected by oxidative insult and PARP-1 inhibition in 661W cells

In order to determine the biological processes affected by the oxidative insult on 661W cells, the common phosphopeptides up-regulated (showing FC ≥ 1) in both H_2O_2 and H_2O_2 + PJ34 treatments were selected for gene ontology (GO) analysis using ClueGO (a GO enrichment bioinformatic tool). This tool distributes the phosphopeptides belonging to a certain GO Biological Process into functional groups. From a total of 445 common up-regulated phosphopeptides in both treatments, the functional group showing higher GO enrichment was *Cellular response to DNA damage stimulus*, followed by *mRNA processing* (Fig. 5B). Therefore, this GO enrichment study showed that the oxidative treatment, both in absence or presence of PJ34, affected mainly the phosphorylation of proteins involved in the cellular response to the DNA damage suggesting that a considerable DNA damage was caused in the 661W cells by OxS.

We also compared between them the GOs enriched in the sets of phosphopeptides up-regulated in H_2O_2 and H_2O_2 + PJ34 treatments (phosphopeptides included in each upper right quadrant of volcano plots in Fig. 5A) using the bioinformatic tool DAVID functional annotation chart (Huang da et al., 2009). For this, up-regulated phophopeptides were linked with the names of their coding genes using the *UniProt Knowledgebase (*https://www.uniprot.org/). Then, the annotations in the GO database were used to allocate the gene names into the corresponding category of Biological

Process terms. The most relevant and over-represented GO Biological Process terms appearing in our analysis were: *Regulation of transcription, DNA-templated*; *Cell cycle*; *Cellular response to DNA damage stimulus; Protein phosphorylation*; *DNA repair*; *Cell division*; and *Apoptotic process* (Fig. 5C).

In addition, the H_2O_2 + PJ34 condition, when compared to H_2O_2, presented more over-phosphorylated proteins (referred to Uniprot ID in Table 1) in categories linked to DDR including *Cell cycle*, *Cellular response to DNA damage* stimulus, *DNA repair* and *Apoptotic process.* As an example, the phosphoprotein ATM (highlighted in Table 1) was up-regulated in H_2O_2 + PJ34 but not in H_2O_2; so, Supplementary Table 1 (Appendix B) shows that the particular phosphopeptide Atm pS1987 was up-regulated in H_2O_2 + PJ34 but not in H_2O_2 conditions. The histone phosphorylation of H2AX was also differentially up-regulated in H_2O_2 + PJ34 (Table 1).

These data suggest that the inhibition of PARP-1 increased the response to DNA damage triggered by H_2O_2 treatment in mitotic 661W cells, similar to what happens in post-mitotic photoreceptor cells in retinal explants (Fig. 3A and B).

3.4. PARP-1 inhibition increases the phosphorylation of proteins at SQ motifs after oxidative treatment

As previously mentioned, 445 phosphopeptides were commonly up-regulated in both treatments when compared to untreated cells; of them 31 were significantly increased in H_2O_2 + PJ34 with respect to H_2O_2, while 9 were decreased for the same comparison. The phosphorylation sites and motifs in these 40 phosphopeptides are listed in Supplementary Table 2 (Appendix B).

The SQ motif was the sequence most frequently phosphorylated in the phosphopeptides differentially expressed in H_2O_2 + PJ34 *versus* H_2O_2 (Fig. 6A and

Supplementary Table 2 in Appendix B). In fact, 61.3% (19/31) of the phosphopeptides significantly increased in H_2O_2 + PJ34 *versus* H_2O_2 were phosphorylated at SQ motifs (Fig. 6B, and Supplementary Table 2 in Appendix B), and included phosphorylations in crucial proteins of the DDR pathway, like BRCA1 and MDC1 (Fig. 6C), and others SQ proteins (Supplementary Fig. 3 in Appendix B). In contrast, none of the 9 phosphopeptides increased in H_2O_2 respect to H_2O_2 + PJ34 were phosphorylated at SQ motifs (Supplementary Table 2 in Appendix B).

Therefore, we demonstrate for the first time using a phosphoproteomic analysis by LC-MS/MS that the inhibition of PARP-1 during the oxidative damage induced by H_2O_2 on a photoreceptor cell line increased the phosphorylation levels of proteins related to DDR.

3.5. Inhibition of PARP-1 activity slowed the cell cycle at G_2/M phase and reduced cell growth after oxidative treatment in 661W cells

The inhibition of PARP-1 during an oxidative insult increased the phosphorylation of some regulators of the DDR, a pathway closely related to the control of the cell cycle in proliferative cells. Thus, we analyzed the cell cycle of 661W cells subjected to the oxidative treatment in presence of PJ34. Flow cytometry analysis revealed a significant increase of cells in the G_2/M phases 24 h after the oxidative insult (from 25.2% of cells in control experiments to 39.0% after H_2O_2 treatment, see Fig. 7A, first and third panels). This increase was still greater when PARP-1 inhibitor was used (percentage of cells in G_2/M phase = 56.7%, see fourth panel in Fig. 7A). Therefore, the oxidative treatment provoked that a proportion of cells arrest at G_2/M their progression in the cell cycle and do not complete their mitosis; this arrest is still greater when PARP-1 is inhibited.

Next, we tested if the arrest of cells at G_2/M detected at 24 h after oxidative treatment was accompanied by a progressive decrease of cell number. SRB assay showed that cell density significantly decreased in a time-dependent manner after H_2O_2 treatment (Fig. 7B), and PARP-1 inhibition by PJ34 produced an additional significant reduction in the growth of oxidative stressed 661W cells.

3.6. Inhibition of PARP-1 activity increases the phosphorylation of ATM/ATR substrates after oxidative insult in both proliferative and post-mitotic retinal cells

To confirm the increase of the phosphorylation of DDR-related proteins in oxidative stressed retinal cells after inhibition of PARP-1, we performed Western blot analysis using a mix of antibodies against ATM/ATR substrates phosphorylated on SQ motifs. We examined first that the oxidative treatment (1 mM of H_2O_2 for 30 min followed by 6 h recovery) produced an increase in the expression of proteins with phosphorylation at SQ motifs in lysates from mitotic cells (661W cells); the level of phosphorylation further increased when the activity of PARP-1 was inhibited (Fig. 8A and B). The blockade of PARP-1 activity in explants (post-mitotic cells) subjected to OxS (3.5 mM of H_2O_2 for 30 min followed by 12 h of recovery) also resulted in higher expression of phosphorylated ATM/ATR substrates (Fig. 8C). Although in this case the densitometry data showed that the phosphorylation of ATM/ATR substrates increased in H_2O_2 + PJ34 conditions (Fig. 8D), the differences between the experimental conditions did not reach significance, perhaps due to the presence in the explants of cells of all retinal layers showing different degree of phosphorylation in response to the treatments.

In summary, these data confirm that the inhibition of PARP-1 after an OxS raises the phosphorylation of proteins at SQ motifs in both mitotic and post-mitotic retinal

cells, probably by increasing the activity of ATM/ATR kinases and other proteins involved in DDR.

4. Discussion

Determination of the phosphorylation level of proteins is of major interest because their function frequently depends on their phosphorylation status. In this regard, the DDR is a signaling pathway that involves the phosphorylation of proteins that participate in the preservation of the genome stability of cells (e.g., DNA repair, cell cycle control, and apoptosis); this pathway is activated by oxidative insults generating high ROS levels that damage the DNA (Jackson and Bartek, 2009; Minchom et al., 2018; Polo and Jackson, 2011). These phenomena were studied by analyzing: (i) DNA damage markers such as phosphorylated histone γ-H2AX, (ii) DDR components such as substrates of kinases ATM and ATR, and determining their activation according to their phosphorylation level, (iii) apoptotic cells, and (iv) cell cycle phases.

Taken together, the results revealed profound changes in the phosphorylation pattern of retinal cells after oxidative treatment with H_2O_2, which became more marked when the activity of PARP-1 (enzyme involved in DNA break repair after oxidative damage) was inhibited. A large part of the γ-H2AX and TUNEL staining in retinal explants was localized in the ONL, indicating that DNA damage and cell death was exacerbated in the photoreceptor layer. Thus, we next performed a detailed phosphoproteomic analysis on the effects of PARP-1 inhibition on the regulation of proteins involved in these processes in oxidative-stressed retinal cells. As the retina is a non-homogenous complex of cells, we selected 661W cells (a cell line showing some traits of retinal photoreceptors) for the purpose of elucidating the changes in protein phosphorylation in oxidative stressed cells when PARP-1 is inhibited.

4.1. Response of 661W cells to DNA damage after H_2O_2 treatment

The treatment of 661W cells with H_2O_2 is a recognized *in vitro* model of photoreceptor oxidative damage (Kunchithapautham and Rohrer, 2007). H_2O_2 induces DNA breaks, and the damaged cells then activate DNA damage signaling and repair pathways to counter these lesions and prevent the transmission of lesions to daughter cells (Hoeijmakers, 2001). After activation of the DDR pathway, hundreds of proteins, including γ-H2AX protein, are phosphorylated on SQ motifs and additional sites by ATM or ATR kinases (Marechal and Zou, 2013).

In this way, our exposure of 661W cells to 1 mM H_2O_2 for 30 min produced a slight increase in ATM phosphorylation at S1987, which was greater (FC ≥ 1) in the presence of the PARP-1 inhibitor (Table 1). It was previously reported that murine ATM becomes activated by phosphorylation at Ser-1987 (Pellegrini et al., 2006), and our phosphoproteomic analysis revealed activation of ATM after H_2O_2 + PJ34 treatment. Given that ATM responds primarily to DNA double-strand breaks (DSBs) (Paull, 2015) and that ATM activation by phosphorylation at Ser-1987 is increased when PARP-1 is inhibited, we hypothesize that PARP-1 inhibition potentiates the generation of DSBs in cells suffering an oxidative damage.

As previously mentioned, one of the substrates of ATM is the histone H2AX, which is phosphorylated at Ser-139 (γ-H2AX) (Podhorecka et al., 2010) and facilities recruitment to the damaged DNA area of proteins that participate in the DDR. Therefore, γ-H2AX is considered as a marker of DSBs in the DNA as well as participating in other biological processes such as the activation of cell cycle checkpoints (Savic et al., 2009; Turinetto and Giachino, 2015). We found a significant increase in the phosphorylation of H2AX at S140 when PARP-1 is inhibited (S140 corresponds to pS139 in the *UniProt* database, which considers the initiation methionine as the first amino acid of the protein).

BRCA1 and MDC1 were among the 19 proteins showing increased phosphorylation at SQ motifs when PJ34 inhibitor was added to the H_2O_2 treatment of 661W cells; both are crucial proteins in the response to DNA damage and cell cycle regulation. BRCA1 and MDC1 are phosphorylated at serine and/or tyrosine residues by ATM/ATR kinases (Traven and Heierhorst, 2005). BRCA1 is phosphorylated by ATM in response to DSBs and by ATR in response to other lesions (Gatei et al., 2001). Our phosphoproteomic study revealed that BRCA1 was phosphorylated on serine at position 1422 (Brca1 pS1422 phosphopeptide). This modification has been related to the function of BRCA1 as regulator of the arrest of cell cycle at G_2/M phase (Traven and Heierhorst, 2005; Xu et al., 2002), consistent with our finding that PARP-1 inhibition potentiates the G_2/M cell cycle arrest induced by H_2O_2. In addition, MDC1 was phosphorylated on serine at position 975 (Mdc1 pS975 phosphopeptide) and threonine at position 325 (Mdc1 pT325 phosphopeptide), although the precise phosphorylation sites of ATM/ATR kinases on MDC1 have not been identified (Traven and Heierhorst, 2005).

In summary, phosphoproteomic analysis reveals an increase in the phosphorylation of proteins associated with the cellular response to oxidative DNA damage (e.g., ATM, BRCA1, MDC1, and H2AX) when PARP-1 is inhibited in 661W cells.

4.2. Mechanisms of PARP-1 potentiating DNA damage after oxidative treatment of 66W cells and retinal explants.

Oxidative damage (e.g., by H_2O_2 treatment) induces both SSBs and DSBs. H_2O_2 preferentially induces SSBs at intermediate concentrations (around 0.5 mM), while DSBs alone are produced at higher concentrations (≥ 50 mM) (Dahm-Daphi et al., 2000; Driessens et al., 2009). Although some response to DSBs cannot be ruled out

(Beck et al., 2014), SSBs are primarily detected by PARP-1, which binds to DNA strand breaks and induces poly-ADP-ribosylation of itself and of other proteins that participate in DNA repair (De Vos et al., 2012; Morgan et al., 2014). In contrast, DSBs induce the phosphorylation of ATM, triggering the phosphorylation of proteins such as BRCA1 and MDC1.

Hence, the oxidative damage produced by our H_2O_2 treatment (3.5 mM for 30 min in explants and 1 mM for 30 min in 661W cells) should predominantly induce SSBs in the DNA; however, unrepaired SSBs may promote DSBs damage after replication or transcription of the DNA (Lindahl, 1993; Woodbine et al., 2011). Thus, the inhibition of PARP-1, which reduces the repair of SSBs, would result in the formation of DSBs and increase the susceptibility of cells to H_2O_2-induced DNA damage (Smith et al., 2016). Interestingly, Aguilar-Quesada et al. (2007) demonstrated that inhibition of PARP-1 activity induces the formation of DSBs and activates ATM to repair the DNA damage produced by γ-irradiation.

We hypothesize that the generation of multiple SSBs induced by 1 mM of H_2O_2 produces an early activation of PARP-1 in 661W cells (Fig. 4), as previously described in another cell line (Martin-Guerrero et al., 2017). Part of this initial damage is not repaired when PARP-1 is inhibited, generating DSBs, a more severe DNA lesion (see Fig. 9A). The ensuing activation of ATM triggers the activation of other proteins in the DDR pathway, finally resulting in G_2/M cell cycle arrest and a decrease in cell survival due to a failure of oxidative damage repair. However, we cannot rule out another type of relationship between PARP-1 and ATM, given reports of functional crosstalk between them. In this context, Watanabe et al. (2004) suggested that PARP-1 negatively regulates ATM kinase activity in response to DSBs, and Aguilar-Quesada et al. (2007) demonstrated that PARP-1 inhibition results in ATM activation. In the same

line, the present study suggests that PARP-1 inhibition after an oxidative damage produces the activation of ATM kinase, increasing the phosphorylation of DDR pathway components (Fig. 9B). At any rate, PARP-1 activation would directly or indirectly regulate ATM activity and consequently the DDR cascade. Further studies are necessary to elucidate whether the increased ATM activity under PARP-1 inhibition is caused by an increase in DSBs or by functional crosstalk between the two proteins.

As depicted in Fig. 7, PARP-1 inhibition blocked cell cycle progression in proliferating 661W cells; however, the relevance of this for non-dividing post-mitotic neurons in the retina is uncertain. We hypothesize that the cell death induced by oxidative treatment in post-mitotic retinal cells would be preceded by the attempt of neurons to re-enter the cell cycle, as observed in various diseases (e.g. in Alzheimer's disease) and when neurons are subjected to acute insults such as oxidative stress (Frade and Ovejero-Benito, 2015). The progression of these neurons in cell cycle is normally blocked; therefore, they do not divide and consequently die by apoptosis, in what is known as "abortive cell cycle re-entry" (Becker and Bonni, 2004). This death apparently involves molecular mechanisms similar to these observed in the response to DNA damage (Frade and Ovejero-Benito, 2015) in which ATM participates (Folch et al., 2012). In this regard, it has been reported that some post-mitotic photoreceptors reactivate proteins involved in the regulation of cell cycle during apoptosis in neurodegenerative diseases (Zencak et al., 2013). We propose that some post-mitotic cells attempt to re-enter the cell cycle after the oxidative treatment of retinal explants, and undergo an abortive process that results in apoptosis. The presence of PJ34 would produce an additional blocking of cell cycle progression, exacerbating cell cycle

arrest and producing more frequent apoptotic cell death, as shown in Figure 2. Further research is warranted to elucidate this issue.

4.3. PARP-1 and photoreceptor degeneration after oxidative damage

The aim of our oxidative treatment with H_2O_2 on retinal explants and 661W cells was to reproduce the OxS of photoreceptor cells during the development of retinal diseases (Nishimura et al., 2017). Insults that damage photoreceptor cells (e.g., light exposure) are known to result in OxS that produces DNA damage, lipid peroxidation, and protein nitrotyrosilation (Lohr et al., 2006), which have all been observed in cones after rod degeneration in models of retinitis pigmentosa (Shen et al., 2005). According to the present findings, PARP-1 inhibition after H_2O_2 treatment increases DNA damage, as reflected in the phosphorylation of proteins involved in DDR, and it reduces cell survival in both retinal explants and 661W cells. This suggests that the DDR pathway culminates in a degenerative process in the presence of a PARP-1 inhibitor. Therefore, the inhibition of PARP-1 enzyme may increase the loss of photoreceptors in retinal diseases associated with an exacerbated OxS. Our observations therefore suggest that PARP-1 activity is necessary to keep cell damage at low levels after an oxidative insult. Consistent with this proposition, our group previously found that oxidative damage in the developing postnatal retina was higher when PARP-1 activity was lower (Martin-Oliva et al., 2015).

It has also been proposed that over-activation of PARP enzymes may contribute to photoreceptor cell death in mice with inherited retinal degeneration (Pearl et al., 2015). This proposal is in line with reports that excessive PARP-1 activation induces cell death, considering the PAR polymer as potentially neurotoxic (Andrabi et al., 2006; Aredia and Scovassi, 2014), and that excessive consumption of NAD^+, a PARP-

1 substrate, depletes ATP in cells, leading to their energy failure (Kauppinen and
2 Swanson, 2007). Hence, PARP-1 activation may exert contrasting effects, being
3 involved in both cell death and DNA repair.

4 Various researchers have observed that a lessening of PARP-1 activity in retinas
5 with inherited degeneration reduces the loss of photoreceptor cells (Paquet-Durand et
6 al., 2007; Sahaboglu et al., 2016). Discrepancies with the present study may be
7 related to the stimulus used to induce cell degeneration. The above authors used
8 experimental models of inherited degeneration of photoreceptors, whereas we studied
9 models (retinal explants and 661W cells) in which an OxS was induced. The same
10 authors state that the efficacy of PARP enzyme inhibition to rescue photoreceptors
11 depended on the mutation responsible for the photoreceptor degeneration (Jiao et al.,
12 2016), indicating that the same mechanisms do not underlie all degeneration
13 processes.

14 Furthermore, it is likely that in experimental models of hereditary degeneration, the
15 mutation-induced primary cell death of rod photoreceptors would not be related to
16 OxS, while oxidative damage would play an important role in the secondary
17 degeneration of cone cells. It should be taken into account that rod photoreceptor
18 degeneration is known to be the direct consequence of genetic mutations, but the true
19 cause of cone cell death has not been established (Narayan et al., 2016). It has been
20 proposed the loss of rod cells produces an increase in oxygen that causes OxS in
21 cone cells, eventually causing their death (Campochiaro and Mir, 2018). Our model,
22 triggered by oxidative damage, is likely related to the secondary death of cone cells
23 described above, showing that PARP-1 inhibition potentiates the oxidative damage
24 and promotes cell death. In this line, Smith et al. (2016) found that PARP-1 inhibition
25 rendered human lens cells more susceptible to H_2O_2-induced DNA strand breaks.

In conclusion, this study shows that the inhibition of PARP-1 during an oxidative insult to retinal cells increases the phosphorylation of multiple proteins related to DDR. A decrease in cell growth (661W cells) and an increase in cell death (retinal explants) was also observed with PARP-1 inhibition. According to the results obtained in *ex vivo* retinal explants and a cone-like photoreceptor cell line, inhibition of PARP-1 reduces cell survival in retinal processes associated with oxidative damage. This finding should be borne in mind when considering the therapeutic use of PARP-1 inhibitors in retinal diseases associated with OxS.

Funding

This work was supported by grants from Ministerio de Educación, Cultura y Deporte, Spain (grant FPU14/02219 and EST16/00301). Work in Pedro R. Cutillas laboratory (London, UK) was funded from Biotechnology and Biological Sciences Research Council (BBSRC, grant BB/M006174/1), Cancer Research UK (CRUK, grant C15966/A24375) and Barts and The London Charity (grant 297/2249). The funding organizations did not participate in the design, execution of the experimental work or writing of this report.

Conflict of interest

No conflict of interest exits for any author.

Acknowledgements

The authors thank Vinothini Rajeeve (mass spectrometrist at Barts Cancer Institute, Queen Mary University of London) for her valuable assistance with mass spectrometry experiments, and Richard Davies for proofreading the English-language manuscript.

References

Aguilar-Quesada, R., Munoz-Gamez, J.A., Martin-Oliva, D., Peralta, A., Valenzuela, M.T., Matinez-Romero, R., Quiles-Perez, R., Menissier-de Murcia, J., de Murcia, G., Ruiz de Almodovar, M., Oliver, F.J., 2007. Interaction between ATM and PARP-1 in response to DNA damage and sensitization of ATM deficient cells through PARP inhibition. BMC molecular biology 8, 29.

Andrabi, S.A., Kim, N.S., Yu, S.W., Wang, H., Koh, D.W., Sasaki, M., Klaus, J.A., Otsuka, T., Zhang, Z., Koehler, R.C., Hurn, P.D., Poirier, G.G., Dawson, V.L., Dawson, T.M., 2006. Poly(ADP-ribose) (PAR) polymer is a death signal. Proceedings of the National Academy of Sciences of the United States of America 103, 18308-18313.

Aredia, F., Scovassi, A.I., 2014. Poly(ADP-ribose): a signaling molecule in different paradigms of cell death. Biochemical pharmacology 92, 157-163.

Beck, C., Robert, I., Reina-San-Martin, B., Schreiber, V., Dantzer, F., 2014. Poly(ADP-ribose) polymerases in double-strand break repair: focus on PARP1, PARP2 and PARP3. Experimental cell research 329, 18-25.

Becker, E.B., Bonni, A., 2004. Cell cycle regulation of neuronal apoptosis in development and disease. Progress in neurobiology 72, 1-25.

Bindea, G., Mlecnik, B., Hackl, H., Charoentong, P., Tosolini, M., Kirilovsky, A., Fridman, W.H., Pages, F., Trajanoski, Z., Galon, J., 2009. ClueGO: a Cytoscape plug-in to decipher functionally grouped gene ontology and pathway annotation networks. Bioinformatics 25, 1091-1093.

Caldecott, K.W., 2008. Single-strand break repair and genetic disease. Nature reviews. Genetics 9, 619-631.

Caldecott, K.W., 2014. Protein ADP-ribosylation and the cellular response to DNA strand breaks. DNA repair 19, 108-113.

Campochiaro, P.A., Mir, T.A., 2018. The mechanism of cone cell death in Retinitis Pigmentosa. Progress in retinal and eye research 62, 24-37.

Casado, P., Wilkes, E.H., Miraki-Moud, F., Hadi, M.M., Rio-Machin, A., Rajeeve, V., Pike, R., Iqbal, S., Marfa, S., Lea, N., Best, S., Gribben, J., Fitzgibbon, J., Cutillas, P.R., 2018. Proteomic and genomic integration identifies kinase and differentiation determinants of kinase inhibitor sensitivity in leukemia cells. Leukemia.

Cutillas, P.R., Vanhaesebroeck, B., 2007. Quantitative profile of five murine core proteomes using label-free functional proteomics. Molecular & cellular proteomics : MCP 6, 1560-1573.

D'Amours, D., Desnoyers, S., D'Silva, I., Poirier, G.G., 1999. Poly(ADP-ribosyl)ation reactions in the regulation of nuclear functions. The Biochemical journal 342 (Pt 2), 249-268.

Dahm-Daphi, J., Sass, C., Alberti, W., 2000. Comparison of biological effects of DNA damage induced by ionizing radiation and hydrogen peroxide in CHO cells. International journal of radiation biology 76, 67-75.

Dantzer, F., de La Rubia, G., Menissier-De Murcia, J., Hostomsky, Z., de Murcia, G., Schreiber, V., 2000. Base excision repair is impaired in mammalian cells lacking Poly(ADP-ribose) polymerase-1. Biochemistry 39, 7559-7569.

De Vos, M., Schreiber, V., Dantzer, F., 2012. The diverse roles and clinical relevance of PARPs in DNA damage repair: current state of the art. Biochemical pharmacology 84, 137-146.

Doonan, F., Wallace, D.M., O'Driscoll, C., Cotter, T.G., 2009. Rosiglitazone acts as a neuroprotectant in retinal cells via up-regulation of sestrin-1 and SOD-2. Journal of neurochemistry 109, 631-643.

Driessens, N., Versteyhe, S., Ghaddhab, C., Burniat, A., De Deken, X., Van Sande, J., Dumont, J.E., Miot, F., Corvilain, B., 2009. Hydrogen peroxide induces DNA single- and double-strand breaks in thyroid cells and is therefore a potential mutagen for this organ. Endocrine-related cancer 16, 845-856.

Duan, W.R., Garner, D.S., Williams, S.D., Funckes-Shippy, C.L., Spath, I.S., Blomme, E.A., 2003. Comparison of immunohistochemistry for activated caspase-3 and cleaved cytokeratin 18 with the TUNEL method for quantification of apoptosis in histological sections of PC-3 subcutaneous xenografts. The Journal of pathology 199, 221-228.

Ferrer-Martin, R.M., Martin-Oliva, D., Sierra, A., Carrasco, M.C., Martin-Estebane, M., Calvente, R., Marin-Teva, J.L., Navascues, J., Cuadros, M.A., 2014. Microglial cells in organotypic cultures of developing and adult mouse retina and their relationship with cell death. Experimental eye research 121, 42-57.

Fisher, A.E., Hochegger, H., Takeda, S., Caldecott, K.W., 2007. Poly(ADP-ribose) polymerase 1 accelerates single-strand break repair in concert with poly(ADP-ribose) glycohydrolase. Molecular and cellular biology 27, 5597-5605.

Folch, J., Junyent, F., Verdaguer, E., Auladell, C., Pizarro, J.G., Beas-Zarate, C., Pallas, M., Camins, A., 2012. Role of cell cycle re-entry in neurons: a common apoptotic mechanism of neuronal cell death. Neurotoxicity research 22, 195-207.

Frade, J.M., Ovejero-Benito, M.C., 2015. Neuronal cell cycle: the neuron itself and its circumstances. Cell cycle 14, 712-720.

Gatei, M., Zhou, B.B., Hobson, K., Scott, S., Young, D., Khanna, K.K., 2001. Ataxia telangiectasia mutated (ATM) kinase and ATM and Rad3 related kinase mediate phosphorylation of Brca1 at distinct and overlapping sites. In vivo assessment using phospho-specific antibodies. The Journal of biological chemistry 276, 17276-17280.

Grasl-Kraupp, B., Ruttkay-Nedecky, B., Koudelka, H., Bukowska, K., Bursch, W., Schulte-Hermann, R., 1995. In situ detection of fragmented DNA (TUNEL assay) fails to discriminate among apoptosis, necrosis, and autolytic cell death: a cautionary note. Hepatology 21, 1465-1468.

Ha, H.C., Snyder, S.H., 1999. Poly(ADP-ribose) polymerase is a mediator of necrotic cell death by ATP depletion. Proceedings of the National Academy of Sciences of the United States of America 96, 13978-13982.

Hoeijmakers, J.H., 2001. Genome maintenance mechanisms for preventing cancer. Nature 411, 366-374.

Hornbeck, P.V., Zhang, B., Murray, B., Kornhauser, J.M., Latham, V., Skrzypek, E., 2015. PhosphoSitePlus, 2014: mutations, PTMs and recalibrations. Nucleic acids research 43, D512-520.

Huang da, W., Sherman, B.T., Lempicki, R.A., 2009. Systematic and integrative analysis of large gene lists using DAVID bioinformatics resources. Nature protocols 4, 44-57.

Iloki-Assanga, S.B., Lewis-Lujan, L.M., Fernandez-Angulo, D., Gil-Salido, A.A., Lara-Espinoza, C.L., Rubio-Pino, J.L., 2015. Retino-protective effect of Bucida buceras against oxidative stress induced by H2O2 in human retinal pigment epithelial cells line. BMC complementary and alternative medicine 15, 254.

Jackson, S.P., Bartek, J., 2009. The DNA-damage response in human biology and disease. Nature 461, 1071-1078.

Jiao, K., Sahaboglu, A., Zrenner, E., Ueffing, M., Ekstrom, P.A., Paquet-Durand, F., 2016. Efficacy of PARP inhibition in Pde6a mutant mouse models for retinitis pigmentosa depends on the quality and composition of individual human mutations. Cell death discovery 2, 16040.

Kastan, M.B., Lim, D.S., 2000. The many substrates and functions of ATM. Nature reviews. Molecular cell biology 1, 179-186.

Kauppinen, T.M., Swanson, R.A., 2007. The role of poly(ADP-ribose) polymerase-1 in CNS disease. Neuroscience 145, 1267-1272.

Kunchithapautham, K., Rohrer, B., 2007. Apoptosis and autophagy in photoreceptors exposed to oxidative stress. Autophagy 3, 433-441.

Lindahl, T., 1993. Instability and decay of the primary structure of DNA. Nature 362, 709-715.

Lohr, H.R., Kuntchithapautham, K., Sharma, A.K., Rohrer, B., 2006. Multiple, parallel cellular suicide mechanisms participate in photoreceptor cell death. Experimental eye research 83, 380-389.

Marechal, A., Zou, L., 2013. DNA damage sensing by the ATM and ATR kinases. Cold Spring Harbor perspectives in biology 5.

Martin-Guerrero, S.M., Munoz-Gamez, J.A., Carrasco, M.C., Salmeron, J., Martin-Estebane, M., Cuadros, M.A., Navascues, J., Martin-Oliva, D., 2017. Poly(ADP-ribose)polymerases inhibitors prevent early mitochondrial fragmentation and hepatocyte cell death induced by H2O2. PloS one 12, e0187130.

Martin-Oliva, D., Martin-Guerrero, S.M., Matia-Gonzalez, A.M., Ferrer-Martin, R.M., Martin-Estebane, M., Carrasco, M.C., Sierra, A., Marin-Teva, J.L., Calvente, R.,

Navascues, J., Cuadros, M.A., 2015. DNA damage, poly(ADP-Ribose) polymerase activation, and phosphorylated histone H2AX expression during postnatal retina development in C57BL/6 mouse. Investigative ophthalmology & visual science 56, 1301-1309.

Minchom, A., Aversa, C., Lopez, J., 2018. Dancing with the DNA damage response: next-generation anti-cancer therapeutic strategies. Therapeutic advances in medical oncology 10, 1758835918786658.

Morgan, M.A., Parsels, L.A., Maybaum, J., Lawrence, T.S., 2014. Improving the efficacy of chemoradiation with targeted agents. Cancer discovery 4, 280-291.

Narayan, D.S., Wood, J.P., Chidlow, G., Casson, R.J., 2016. A review of the mechanisms of cone degeneration in retinitis pigmentosa. Acta ophthalmologica 94, 748-754.

Nishimura, Y., Hara, H., Kondo, M., Hong, S., Matsugi, T., 2017. Oxidative Stress in Retinal Diseases. Oxidative medicine and cellular longevity 2017, 4076518.

Paquet-Durand, F., Silva, J., Talukdar, T., Johnson, L.E., Azadi, S., van Veen, T., Ueffing, M., Hauck, S.M., Ekstrom, P.A., 2007. Excessive activation of poly(ADP-ribose) polymerase contributes to inherited photoreceptor degeneration in the retinal degeneration 1 mouse. The Journal of neuroscience : the official journal of the Society for Neuroscience 27, 10311-10319.

Paull, T.T., 2015. Mechanisms of ATM Activation. Annual review of biochemistry 84, 711-738.

Pearl, L.H., Schierz, A.C., Ward, S.E., Al-Lazikani, B., Pearl, F.M., 2015. Therapeutic opportunities within the DNA damage response. Nature reviews. Cancer 15, 166-180.

Pellegrini, M., Celeste, A., Difilippantonio, S., Guo, R., Wang, W., Feigenbaum, L., Nussenzweig, A., 2006. Autophosphorylation at serine 1987 is dispensable for murine Atm activation in vivo. Nature 443, 222-225.

Pellicciari, R., Camaioni, E., Costantino, G., Formentini, L., Sabbatini, P., Venturoni, F., Eren, G., Bellocchi, D., Chiarugi, A., Moroni, F., 2008. On the way to selective PARP-2 inhibitors. Design, synthesis, and preliminary evaluation of a series of isoquinolinone derivatives. ChemMedChem 3, 914-923.

Perkins, D.N., Pappin, D.J., Creasy, D.M., Cottrell, J.S., 1999. Probability-based protein identification by searching sequence databases using mass spectrometry data. Electrophoresis 20, 3551-3567.

Podhorecka, M., Skladanowski, A., Bozko, P., 2010. H2AX Phosphorylation: Its Role in DNA Damage Response and Cancer Therapy. Journal of nucleic acids 2010.

Polo, S.E., Jackson, S.P., 2011. Dynamics of DNA damage response proteins at DNA breaks: a focus on protein modifications. Genes & development 25, 409-433.

Rass, U., Ahel, I., West, S.C., 2007. Defective DNA repair and neurodegenerative disease. Cell 130, 991-1004.

Sahaboglu, A., Barth, M., Secer, E., Amo, E.M., Urtti, A., Arsenijevic, Y., Zrenner, E., Paquet-Durand, F., 2016. Olaparib significantly delays photoreceptor loss in a model for hereditary retinal degeneration. Scientific reports 6, 39537.

Savic, V., Yin, B., Maas, N.L., Bredemeyer, A.L., Carpenter, A.C., Helmink, B.A., Yang-Iott, K.S., Sleckman, B.P., Bassing, C.H., 2009. Formation of dynamic gamma-H2AX domains along broken DNA strands is distinctly regulated by

ATM and MDC1 and dependent upon H2AX densities in chromatin. Molecular cell 34, 298-310.

Schieber, M., Chandel, N.S., 2014. ROS function in redox signaling and oxidative stress. Current biology : CB 24, R453-462.

Schneider, C.A., Rasband, W.S., Eliceiri, K.W., 2012. NIH Image to ImageJ: 25 years of image analysis. Nature methods 9, 671-675.

Schreiber, V., Dantzer, F., Ame, J.C., de Murcia, G., 2006. Poly(ADP-ribose): novel functions for an old molecule. Nature reviews. Molecular cell biology 7, 517-528.

Shannon, P., Markiel, A., Ozier, O., Baliga, N.S., Wang, J.T., Ramage, D., Amin, N., Schwikowski, B., Ideker, T., 2003. Cytoscape: a software environment for integrated models of biomolecular interaction networks. Genome research 13, 2498-2504.

Shen, J., Yang, X., Dong, A., Petters, R.M., Peng, Y.W., Wong, F., Campochiaro, P.A., 2005. Oxidative damage is a potential cause of cone cell death in retinitis pigmentosa. Journal of cellular physiology 203, 457-464.

Shieh, W.M., Ame, J.C., Wilson, M.V., Wang, Z.Q., Koh, D.W., Jacobson, M.K., Jacobson, E.L., 1998. Poly(ADP-ribose) polymerase null mouse cells synthesize ADP-ribose polymers. The Journal of biological chemistry 273, 30069-30072.

Smith, A.J., Ball, S.S., Bowater, R.P., Wormstone, I.M., 2016. PARP-1 inhibition influences the oxidative stress response of the human lens. Redox biology 8, 354-362.

Tan, E., Ding, X.Q., Saadi, A., Agarwal, N., Naash, M.I., Al-Ubaidi, M.R., 2004. Expression of cone-photoreceptor-specific antigens in a cell line derived from

retinal tumors in transgenic mice. Investigative ophthalmology & visual science 45, 764-768.

Traven, A., Heierhorst, J., 2005. SQ/TQ cluster domains: concentrated ATM/ATR kinase phosphorylation site regions in DNA-damage-response proteins. BioEssays : news and reviews in molecular, cellular and developmental biology 27, 397-407.

Turinetto, V., Giachino, C., 2015. Multiple facets of histone variant H2AX: a DNA double-strand-break marker with several biological functions. Nucleic acids research 43, 2489-2498.

Watanabe, F., Fukazawa, H., Masutani, M., Suzuki, H., Teraoka, H., Mizutani, S., Uehara, Y., 2004. Poly(ADP-ribose) polymerase-1 inhibits ATM kinase activity in DNA damage response. Biochemical and biophysical research communications 319, 596-602.

Wilkes, E., Cutillas, P.R., 2017. Label-Free Phosphoproteomic Approach for Kinase Signaling Analysis. Methods in molecular biology 1636, 199-217.

Woodbine, L., Brunton, H., Goodarzi, A.A., Shibata, A., Jeggo, P.A., 2011. Endogenously induced DNA double strand breaks arise in heterochromatic DNA regions and require ataxia telangiectasia mutated and Artemis for their repair. Nucleic acids research 39, 6986-6997.

Xu, B., O'Donnell, A.H., Kim, S.T., Kastan, M.B., 2002. Phosphorylation of serine 1387 in Brca1 is specifically required for the Atm-mediated S-phase checkpoint after ionizing irradiation. Cancer research 62, 4588-4591.

Yamato, S., Hirabayashi, Y., Sugihara, H., 1984. An improved procedure for the histochemical demonstration of cathepsin D by the mercury-labeled pepstatin method. Stain technology 59, 113-120.

Zencak, D., Schouwey, K., Chen, D., Ekstrom, P., Tanger, E., Bremner, R., van Lohuizen, M., Arsenijevic, Y., 2013. Retinal degeneration depends on Bmi1 function and reactivation of cell cycle proteins. Proceedings of the National Academy of Sciences of the United States of America 110, E593-601.

Figure legends

Fig. 1. Graphical representation of the oxidative treatments in absence or presence of the PARP-1 inhibitor PJ34. The upper and bottom panels show oxidative treatments performed on retinal explants and 661W cells, respectively. Black arrows indicate the culture of retinal cells in fresh medium, red arrows the oxidative treatment with H_2O_2 for 30 min (in absence or presence of PARP-1 inhibitor), and blue arrows the incubation with medium supplemented with PJ34 inhibitor. Detailed information about the times of incubation in each experimental procedure is described in Materials and Methods.

Fig. 2. Effects of H_2O_2 treatment and PARP-1 inhibition on mouse retinal explants. A: Toluidine blue stained semithin sections of retinal explants obtained from P12 mice and cultured for 48 h as indicated in Fig. 1. Control explants (left panel) showed a normal morphology with an organized outer (ONL) and inner (INL) nuclear and ganglion cell (GCL) layers. H_2O_2 treated explants (middle panel) showed frequent swollen cells and pyknotic nuclei, indicative of degeneration in the INL and ONL. Similar observations were made in retinal explants treated with H_2O_2 and PJ34 (right panel). Scale bar: 50 µm. B: Confocal microscopy images showing the distribution of TUNEL-positive cells (green color) and active caspase-3 immunolabeling (red color) in retinal explants in response to the treatments indicated in Fig. 1. DAPI staining (blue color) was used to reveal the retinal layers. Images are representative of three different retinal explants per condition. Note as TUNEL staining notably increased 24 h after oxidative treatment in presence of PJ34 inhibitor (3.5 mM H_2O_2 + PJ34) and

colocalized with the immunoreactivity of active caspase-3. Scale bar: 25 µm. C: Counts of TUNEL-positive cells in the ONL (photoreceptor layer) of three fields (at 630x magnification) of three sections as we described in 2.5 Materials and Methods section. Data represent the means ± SEM of three independent experiments. $^{**}P < 0.01$ with respect to control cells and $^{\#}P < 0.05$ with respect to 3.5 mM H_2O_2.

Fig. 3. Detection of γ-H2AX and activation of PARP-1 in retinal explants. A: Confocal microscopy images showing the immunolocalization of γ-H2AX staining (green color) in retinal explants exposed to the conditions indicated in Fig. 1. Nuclei of retinal layers were counterstained with DAPI (blue color). Images are representative of results obtained for three different retinal explants per condition. Note that γ-H2AX immunolabeling is more robust in the ONL in oxidative stressed retinal sections when PARP-1 was inhibited by PJ34. Scale bar: 25 µm. B: Counts of γ-H2AX-positive cells in the ONL (photoreceptor layer) of three fields (at 630x magnification) of three sections as we described in 2.4 Materials and Methods section. Data represent the means ± SEM of three independent experiments. $^{***}P < 0.001$ and $^{**}P < 0.01$ with respect to control cells and $^{\#\#\#}P < 0.001$ with respect to 3.5 mM H_2O_2. C: Representative Western blot showing an increase of PARP-1 activity 12 h after the oxidative treatment. Activation of PARP-1 was measured by detecting the presence of Poly-ADP-ribosylated proteins (PARylated proteins) in protein extracts from retinal explants exposed 30 min to H_2O_2 and left to recovery 12 h in absence or presence of PJ34 inhibitor. PJ34 impaired the Poly-ADP-ribosylation of proteins after oxidative treatment. β-Actin was used as the loading control. Proteins lysate in each sample were

prepared from three retinal explants of different mice and 30 µg of total protein lysate per sample were loaded in the gel.

Fig. 4. PARP-1 activity is an early event in response to oxidative treatment in 661W cells. A: PARP-1 activity was measured by detecting the presence of Poly-ADP-ribosylated proteins (PARylated proteins) by Western blot. H_2O_2 (1 mM) was added to 661W cells (seeded at a density of $1 \cdot 10^6$ cells per well of a six well plate) for 15 or 30 min and then removed. Cell extracts for the detection of PARylated proteins were collected at 0, 15 and 30 min during H_2O_2 exposure and at 15 min, 2 and 6 h after H_2O_2 removal (15, 120 and 360 min of post-incubation time). β-Tubulin was used as loading control. Thirty µg of total protein lysate per sample were loaded in the gel. B: Cells (seeded at a density of $1 \cdot 10^6$ cells) were treated with 1 mM H_2O_2 for 15 min in absence or presence of the PARP-1 inhibitor PJ34 (1 µM) and then PARylated proteins were detected. β-Actin was used as loading control. Thirty µg of total protein lysate per sample were loaded in the gel. C: Representative immunofluorescence images showing the presence of Poly-ADP-ribose polymer (PAR, green color) upon oxidative treatment. Cells were treated for 15 min with 1 mM H_2O_2 in absence or presence of 1 µM PJ34. Nuclei were stained with Hoechst (blue color). Scale bar: 50 µm.

Fig. 5. Determination of subsets of phosphopeptides significantly up-regulated after treatment with H_2O_2 in 661W cells and identification of their biological functions. A: Phosphopeptides identified by LC-MS/MS were represented in a volcano plot according to their statistical *P* value (-Log *P* value, y axis) and their Fold Change (FC = Log_2 Ratio, x axis). Left panel (H_2O_2) shows the volcano plot

of 661W cells treated with 1 mM H_2O_2 for 30 min and then incubated for 6 h in fresh medium compared to control untreated cells, and right panel (H_2O_2 + PJ34) shows cells treated with H_2O_2 and PJ34 (1 μM) and post-incubated for 6h (in the presence of PJ34) compared to control cells. Horizontal and vertical dashed lines indicate the filtering criteria (P = 0.05 and FC = ± 1.0, respectively). Red dots correspond to phosphopeptides that change significantly in experimental conditions respect to control (P < 0.05; dots above the horizontal dashed line) while gray dots represent phosphopetides showing no significant changes (P > 0.05; dots below the horizontal dashed line). The number of up-regulated (FC ≥ 1) phosphopeptides (pp) is shown above the upper right rectangle in each plot. B: Gene ontology (GO) enrichment analysis chart showing the functional groups linked to the common up-regulated phosphopeptides in both H_2O_2 and H_2O_2 + PJ34 treatments compared to control. GO enrichment analysis was carried out using ClueGO. Only significant functional groups are showed (**P < 0.01). C: Graphical representation of Biological Processes associated to the phosphopeptides up-regulated in H_2O_2 or H_2O_2 + PJ34 treatments *versus* control (phosphopeptides represented in the upper right quadrant in both plots in A). DAVID Bioinformatics analyses were performed to determine GO enrichment for Biological Process terms. Each bar graph represents the number of genes corresponding to each term; only the more populated terms in both experimental conditions (i.e. terms associated with more genes) are represented.

Fig. 6. Phosphopeptides differentially expressed between 661W cells treated with H_2O_2 in presence of PARP-1 inhibitor (H_2O_2 + PJ34) and cells treated with H_2O_2 only (H_2O_2). A: Sequence logo plot of the motif analysis for the 40 up-regulated

phosphopeptides differentially expressed in H_2O_2 + PJ34 versus H_2O_2 treatments. The chart represents the most frequent amino acids surrounding the phosphorylated residue. The relative position of the residues in the motif is shown on the X-axis ("N" refers to amino-terminal and "C" to carboxy-terminal) and the size of the amino acid symbol is proportional to the frequency of each residue in the motifs. The phosphorylated amino acid residue occupies position 0. Note that the residues most represented are those of serine (S) in position 0 and glutamine (Q) in position 1. B: Graphical representation of the Fold Change (FC) values of the 19 differentially up-regulated phosphopeptides showing phosphorylation at SQ motifs in H_2O_2 + PJ34 and H_2O_2 treatments. C: Signal intensity histograms detected by LC-MS/MS for the phosphopeptides Brca1 pS1422 and Mdc1 pS975. These peptides are phosphorylated at SQ motifs and included in the subset represented in section B. The y axis represents the normalized signal intensity obtained by LC-MS/MS analysis (mean values ± SEM) for each treatment (n= 4). ***$P < 0.001$ respect to control; $^{\#\#}P < 0.01$ respect to H_2O_2 treatment.

Fig. 7. Effect of inhibiting PARP-1 under oxidative conditions on cell cycle and cell growth. A: Representative plots for propidium iodide staining showing the cell cycle phases distribution of 661W cells exposed to oxidative stress and PARP-1 inhibition with PJ34 as indicated in Fig 1. The percentage of cells (± SEM) in each phase of cell cycle obtained from flow cytometric analysis in three independent experiments is indicated on bottom of the plots. *$P < 0.05$ for each treatment compared to control for the respective cell cycle phase; $^{\#}P < 0.05$ for oxidative treatment with PJ34 compared to oxidative treatment without PJ34. B: Survival curve representing the number of 661W cells after the oxidative treatment. Cells

were exposed to 1 mM H_2O_2 for 30 min in the presence or absence of PARP-1 inhibitor PJ34 (1 µM) and left to recover 0, 24, 48 and 72 h. In PJ34 treated cells, inhibitor was added 16 h before H_2O_2 and kept during and after the oxidative stress conditions. Cell density was measured using the Sulforhodamine B colorimetric assay in three independent experiments. *P < 0.05 respect to the controls; $^{\#}P$ < 0.05 between both oxidative treatments.

Fig. 8. PARP-1 inhibition during oxidative insult increased the activation of ATM/ATR in retinal cells. A: Representative western blot showing the effects of H_2O_2 treatment and PARP-1 inhibition on the phosphorylation levels of the ATM/ATR substrates in 661W cells. 661W cells were seeded at a density of $1 \cdot 10^6$ cells per well of a six well plate and treated with 1 mM H_2O_2 for 30 min in absence or presence of PJ34, and then incubated in fresh medium (with or without PJ34) for 6 h. The pre-incubation with PJ34 began 16 h before H_2O_2 treatment. Thirty µg of total protein lysate per sample were loaded in the gel. β-Actin was used as loading control. B: Densitometric analysis of phosphorylation of ATM/ATR substrates normalized to β-actin expression of three independent experiments in the conditions described in A. Data were expressed as mean (± SEM) of grey value for a representative band in three independent experiments and relativized to untreated cells signal. PARP-1 inhibition in oxidative stressed cells induced a significant increase (*P < 0.05) in the phosphorylation of ATM/ATR substrates respect to untreated cells. C: Representative Western blot of proteins lysate from three retinal explants obtained from different mice in three independent experiments showing the effects of H_2O_2 treatment and PARP-1 inhibition on the phosphorylation levels of the ATM/ATR substrates. Explants were treated with 3.5

mM H_2O_2 for 30 min in absence or presence of PJ34 and then incubated in fresh medium (with or without PJ34) for 12 h. The pre-incubation with PJ34 began 16 h before H_2O_2 treatment. Thirty µg of a mix of protein lysate from three retinal explants were loaded in each lane of the gel. β-Tubulin was used as loading control. D: Densitometric analysis of phosphorylation of ATM/ATR substrates normalized to β-tubulin expression of three independent experiments in the conditions described in C. Data were expressed as mean (± SEM) of grey value for a representative band in three independent experiments and relativized to untreated explants signal.

Fig. 9. Scheme showing the proposed model by which PARP-1 inhibition potentiates the phosphorylation of DDR proteins induced by ROS in photoreceptor cells. A: inhibition of PARP-1 provokes that unrepaired SSBs transform into DSBs, and in turn induce the activation (phosphorylation) of ATM that phosphorylates proteins of the DDR pathway (including BRCA1 and MDC1), resulting finally in cell cycle arrest (of proliferating retinal cells) and cell death if the lesions are not correctly repaired after H_2O_2 treatment. B: PARP-1 negatively regulates the activation of ATM. Thus, PARP-1 inhibition leads to an increased activation of ATM and an increased phosphorylation of proteins involved in the DDR pathway as described in A.

Table 1

Gene Ontology Biological Process terms and Uniprot ID of up-regulated phosphoproteins (showing a Fold Change ≥ 1) in 661W cells subjected to the oxidative treatment with H_2O_2 (H_2O_2) and to the oxidative treatment in presence of PJ34 inhibitor (H_2O_2 + PJ34). *Unique phosphoproteins up-regulated in each condition.

Regulation of transcription, DNA-templated				Cell cycle				Cellular response to DNA damage stimulus				Protein phosphorylation			
H_2O_2		H_2O_2 + PJ34		H_2O_2		H_2O_2 + PJ34		H_2O_2		H_2O_2 + PJ34		H_2O_2		H_2O_2 + PJ34	
AAPK1	LIMD1*	AAPK1	MED24	ARHG2	MCM6	ARHG2	KS6A3	ASH2L	MYC	ASH2L	MYC	AAK1	NEK9	AAK1	KS6A4
ARI1A	MED24	ARI1A	MYC	BIRC6	MDC1	ASPP2*	LIN54*	ATRX	NBN	**ATM***	NBN	AAPK1	PASK	AAPK1	MAST4*
ASH2L	MYC	ASH2L	MYCB2	BRCA1	NASP	**ATM***	LIN9	BD1L1	NIPBL	ATRX	NIPBL	ARAF	PKN2	ABL2*	NEK9
ATF1	MYCB2	ATF1	NELFE	BRD7	NBN	BIRC6	MCM6	BRCA1	RAD50	BD1L1	OTUB1*	BUB1B*	PP2BB	ARAF	PAK1*
ATRX	NELFE	ATRX	NFAC3	BUB1B*	NEK9	BRCA1	MDC1	CBL	RBBP6	BRCA1	RAD50	CBL	PTK7	**ATM***	PAK2*
BRCA1	NFAC3	BCAS3*	NFAC4	CD2AP	NIPBL	BRD7	NASP	CDC5L	RD23A	CBL	RBBP6	CDK9	RAF1*	CBL	PASK
BRD7	NFAC4	BRCA1	NFIA	CDC5L	PAPD5	CASC5*	NBN	CDK9	RIF1	CDC5L	RD23A	CHK1	RIPK1	CCNE1*	PKN2
BRE1A*	NFIA	BRD7	NFIL3*	CDN1A	PKN2	CCNE1*	NEK9	CDN1A	SMC1A	CDK9	RIF1	CHK2	SIK3	CDK9	PP2BB
CBX3*	P66B	CDC5L	P66B	CEP55	PPM1G	CD2AP	NIPBL	CHK1	SMC3	CDN1A	SMC1A	EPHA2	SLK	CHK1	PTK7
CDC5L	PB1	CDK9	PB1	CHK1	RAD50	CDC23*	PAPD5	CHK2	TERA	CHK1	SMC3	GSK3A	STK10	CHK2	RIPK1
CDK9	PININ	CDYL	PHF2*	CHK2	RAN	CDC5L	PKN2	COM1	TOPB1	CHK2	TERA	ILF3	TIF1B	CREB1*	RIPK3*
CDYL	PKN2	CEBPD	PININ	CLAP1	RIF1	CDN1A	PPM1G	DTL	TOPRS*	COM1	TOPB1	KPCD2	ULK1	EPHA2	SIK3
CEBPD	PML	CHD1	PKN2	CLAP2*	SMC1A	CEP55	RAD50	F175A	TP53B	DTL	TP53B	KS6A1	VRK1	GSK3A	SLK
CHD1	PSIP1	CHD8	PML	COM1	SMC3	CHK1	RAN	MDC1	UBA1	F175A	TYY1*	KS6A3	WNK1*	ILF3	STK10
CHD8	RBM14	CHK2	PSIP1	CTDP1	STA13	CHK2	RIF1	MSH6	XRCC6	**H2AX***	UBA1	KS6A4		KC1E*	TIF1B
CHK2	RBM39	COPRS	PTRF*	DIXC1*	STAG2	CLAP1	SMC1A	MUM1		MDC1	XRCC6			KPCD2	ULK1
COPRS	REQU	CREB1*	RBM14	EP300	STK10	COM1	SMC3			MSH6				KS6A1	VRK1
CRTC2	RHG35	CRTC2	RBM39	INCE*	TPR	CTDP1	STA13			MUM1				KS6A3	
CUX1	RUNX2	CUX1	REQU	KIF23	VRK1	EP300	STAG2								
DDX17	SAFB1	DDX17	RHG35	KS6A3	ZW10*	ERC6L*	STK10								
DNMT1	SAFB2	DNMT1	RUNX2	LIN9		**H2AX***	TPR								
DSRAD	SBNO1	DSRAD	SAFB1			KIF11*	VRK1								
ELP1	SLTM	ELP1	SAFB2			KIF23									
EP300	SMCA4	EP300	SBNO1												
ETV3	SMRC1	ETV3	SLTM												
FUBP2	SP1	FOXO3*	SMCA4												
GABP2	TDIF2	FUBP2	SMRC1												
HP1B3	TGIF1*	GABP2	SP1												
HTSF1	TIF1B	HDGF*	T22D4*												
I2BP1	TP53B	HP1B3	TDIF2												
I2BP2	TR150	HTSF1	TIF1B												
ILF3	XRCC6	I2BP1	TP53B												
JUNB	YBOX2	I2BP2	TR150												
KAT6A	ZMYM2	ILF3	TYY1*												
KS6A4	ZN148	JUNB	XRCC6												
LBH		KAT6A	YBOX2												
		KS6A4	ZBED6*												
		LBH	ZMYM2												
		LIN54*	ZN148												

DNA repair				Cell division				Apoptotic process			
H_2O_2		H_2O_2 + PJ34		H_2O_2		H_2O_2 + PJ34		H_2O_2		H_2O_2 + PJ34	
ATRX	NBN	**ATM***	NBN	ARHG2	NEK9	ARHG2	KIF23	BIRC6	PML	ASPP2*	PAK2*
BD1L1	PDS5A	ATRX	OTUB1*	BIRC6	PAPD5	BIRC6	MAP4*	BUB1B*	PRUN2	BIRC6	PKN2
BRCA1	RAD50	BD1L1	PDS5A	BUB1B*	PDS5A	CASC5*	NEK9	CHK2	REQU	CHK2	PML
CDC5L	RD23A	BRCA1	RAD50	CD2AP	PKN2	CCNE1*	PAPD5	CLIC4	RIPK1	CLIC4	PRUN2
CDK9	SMC1A	CDC5L	RD23A	CEP55	RAN	CD2AP	PDS5A	EP300	SLK	EP300	REQU
CHK1	SMC3	CDK9	SMC1A	CHK2	SMC1A	CDC23*	PKN2	EPHA2	SLTM	EPHA2	RIPK1
CHK2	TERA	CHK1	SMC3	CLAP1	SMC3	CDC27*	RAN	FAF1	SQSTM	FAF1	SLK
COM1	TIF1B	CHK2	TERA	CLAP2*	STAG2	CEP55	SMC1A	HMOX1	TISB	FOXO3*	SLTM
F175A	TOPB1	COM1	TIF1B	COM1	TPR	CHK2	SMC3	MCL1		HMOX1	SQSM
MDC1	TP53B	F175A	TOPB1	CTDP1	VRK1	CLAP1	SPG20*	PKN2		MCL1	TISB
MSH6	XRCC6	**H2AX***	TP53B	INCE*	ZW10*	COM1	STAG2			PAK1*	
MUM1		MDC1	TYY1*	KIF23		CTDP1	TPR				
		MSH6	XRCC6			ERC6L*	VRK1				
		MUM1				KIF11*					

APPENDIX A. SUPPLEMENTARY MATERIALS AND METHODS

POLY(ADP-RIBOSE) POLYMERASE-1 INHIBITION POTENTIATES CELL DEATH AND PHOSPHORYLATION OF DNA DAMAGE RESPONSE PROTEINS IN OXIDATIVE STRESSED RETINAL CELLS

Sandra M. Martín-Guerrero, Pedro Casado, José A. Muñoz-Gámez, María-Carmen Carrasco, Julio Navascués, Miguel A. Cuadros, Juan F. López-Giménez, Pedro R. Cutillas, David Martín-Oliva

A.1. Mass spectrometry-based phosphoprotemics

Phosproteomics studies were performed using liquid chromatography tandem-mass spectrometry (LC-MS/MS). 661W cells seeded in 150 mm culture dishes were treated for 30 min with 1 mM H_2O_2 and further incubated in fresh medium for 6 h; PARP-1 activity was pharmacologically inhibited as described in Materials and Methods section. Then, cells were processed for phosphoproteomics analysis as already described (Casado et al., 2018; Wilkes and Cutillas, 2017). For that, cells from four independent biological replicates were lysed in urea buffer (8M urea in 20 mM HEPES pH 8.0) containing phosphatase inhibitors (1 mM Na_3VO_4, 1 mM NaF, 1 mM β-glycerol-phosphate and 2.5 mM $Na_4P_2O_7$) and homogenized by sonication (30 cycles of 30 s on 30 s off; Diagenode Bioruptor® Plus, Liege, Belgium). Insoluble material was removed by centrifugation at 16000 g for 10 min at 5 ºC and protein in the cell extracts was quantified by bicinchoninic acid (BCA) analysis. 500 µg of extracted proteins were reduced with DTT (10 mM) for 1 h at 25 ºC and alquilated with Iodoacetamide (IAM, 16.6 mM) for 30 min at 25 ºC. Then, samples were diluted with 20 mM HEPES (pH 8.0) to a final concentration of 2 M urea and digested with equilibrated trypsin beads (100 µl of 50% slurry of TLCK-trypsin per sample; cat # 20230, Thermo Fisher Scientific, Waltham, MA) overnight at 37 ºC. After that, trypsin beads were removed by centrifugation (2000 g for 5 min at 5 ºC) and samples were desalted using OASIS cartridges (10 mg OASIS-HLB cartridges, Waters, Manchester, UK). Columns were activated with acetonitrile (ACN) and equilibrated with a desalting washing solution (1% ACN, 0.1% trifluoroacetic acid, TFA), then, samples were loaded

into the cartridges and washed twice with the desalting washing solution. Finally, peptides were eluted with glycolic solution 1 (1 M Glycolic acid, 50% ACN, 5% TFA) and subjected to phosphoenrichment with TiO_2. Sample volumes were normalized to 1 ml with glycolic solution 2 (1 M Glycolic acid, 80% ACN, 5% TFA) and incubated for 5 min with TiO_2 (50 µl per sample of 500 µg/ml of TiO_2 in 1% TFA). Afterwards, samples were loaded in empty spin tips by centrifugation for 30 s at 1500 g. Samples were sequentially washed by centrifugation with glycolic solution 2 and phosphoenrichment washing solutions 1 (100 mM ammonium acetate in 25% ACN) and 2 (10% ACN). After that, phosphopeptides were eluted 4 times with elution solution (5% NH_4OH). Finally, eluents were snap frozen in dry ice for 15 min, dried in a speed vac overnight and phosphopeptide pellets stored at -80 ºC. Peptide pellets were resuspended in 13 µl of reconstitution buffer (20 fmol/µl enolase in 3% ACN, 0.1% TFA), and 5 µl (from two technical replicates for each biological sample) were loaded in an LC-MS/MS platform consisting in a Dionex UltiMate 3000 RSLC directly coupled to an Orbitrap Q-Exactive Plus mass spectrometer using the Easy-Spray Ion Source (Thermo Fisher Scientific).

Mascot Demon was used to automate the identification of phosphopeptides from MS/MS spectra. Thus, Mascot Distiller (version 2.5.0) was used to generate the peak lists that were used by Mascot search engine (Perkins et al., 1999). Searches were performed against the Swiss-Prot *Mus musculus* database (uniprot_sprot_2014_08.fasta) considering 2 trypsin missed cleavages, mass tolerance of ± 10 ppm for the MS scans and ± 25 mmu for the MS/MS scans, carbamidomethyl Cys as a fixed modification, PyroGlu on N-terminal Gln, oxidation of Met and phosphorylation on Ser, Thr, and Tyr as variable modifications. Pescal was used for quantification of label free phosphopeptides across experimental conditions (Cutillas and Vanhaesebroeck, 2007). For the determination of intensity values, Pescal generated extracted ion chromatograms (XICs)

for all identified phosphopeptides across all conditions and quantified the area from XICs using the parameters described previously (Casado et al., 2018). Data was normalized to the sum of all peptide intensities derived from a sample (column).

To determine phosphorylation changes induced by treatments, the signals from treated cells were divided by those of the respective untreated control samples and given as Fold Changes in Log_2 Ratio. Thus, Fold Change = log_2 Ratio, calculated as mean of normalized phosphopeptide signals across biological replicates in oxidative conditions/mean of normalized phosphopeptide signals across replicates in untreated cells. Two tail unpaired Students t-test and One-way analysis of variance (ANOVA) with Tukey's multiple comparison tests were used to determine if phosphopeptides showed a significant difference between control and oxidative treatment with H_2O_2 and between control and oxidative treatment in presence of PARP-1 inhibitor (H_2O_2 + PJ34 treatment). Significant phosphopeptides (*P* value < 0.05) showing a Fold Change ≥ 1 for any comparisons (H_2O_2 or H_2O_2 + PJ34) were selected and classified as unique (up-regulated only in H_2O_2 or in H_2O_2 + PJ34 treatments) or common (up-regulated in both treatments). Common phosphopeptides that showed a significant Fold Change increase in the H_2O_2 + PJ34 treatment compared to H_2O_2 were considered for further analyses that included motif phosphorylation studies (phosphorylation of SQ motifs). Also, phosphopeptides were ranked in a volcano plot according to their statistical *P* value (-Log *P* value, y-axis) and their Fold Change (log_2 ratio, x-axis) in H_2O_2 and H_2O_2 + PJ34 treatment, both compared to control.

A.2. Functional Gene Ontology analysis

In order to contextualize the phosphoproteomics data obtained and extract valuable information that allows the generation of a hypothesis testable by challenge, the list has to

be further classified and filtered. We selected phosphopeptides with significant (*P* value < 0.05) and representative Fold Changes (1 ≤ Fold Change ≤ -1) between treated (H_2O_2 or H_2O_2 + PJ34) and control cells to perform a Gene Ontology (GO) analysis. The resultant protein identifier list (accession number provided by Mascot search) was linked to its associated GO Biological Process terms with DAVID (Database for Annotation, Visualization and Integrated Discovery) Bioinformatic tool (version 6.8) to identify the most relevant (over-represented) biological terms associated with the previous protein list (Huang da et al., 2009). The threshold value of group membership counts was set at 2 and the EASE score (Modified Fisher's Exact test *P* value) was set at 0.1. Finally, the top of Biological Process terms significantly enriched (showing *P* value < 0.05 for the Modified Fisher's Exact *test*) were selected and represented in a functional chart.

Additionally, the common up-regulated phosphopeptides were selected to perform GO analysis. Proteins comprising the selected peptides were linked to their associated GO Biological Process terms with ClueGO, a plug-in of Cytoscape (v.3.3.0) that ascribe the GO Biological Process terms to functional groups (Bindea et al., 2009; Shannon et al., 2003). To determine GO enrichment, two-sided hyper-geometric distribution tests (enrichment/depletion), followed by the Bonferroni Step Down adjustment was applied to the protein-GO associations created by ClueGO. GO were considered enriched when the corrected *P*-value was ≤ 0.05 and the number of regulated proteins linked to the GO term were higher than 2 or represents more than 4% of the total proteins linked to the term. In order to reduce the redundancy of the terms that have similar associated proteins, the fusion criteria (GO term fusion) was also applied and the Kappa-statistics score threshold was set to 0.3. Also, the GO terms were associated in functional groups using the Kappa score and leading term groups were selected based on the highest significance. The functional grouping was used with an initial group size of 1 and 50% for a group merge.

A.3. Logo sequence motifs analysis

To analyse the most abundant phosphorylation motif of those significant phosphopeptides, we prealigned manually the sequences for each phosphopeptide, where the modification site was centrally located for correct statistical analysis and flanked by 5 residues (a sequence of 11 residues for each phosphosite). Next we generated the sequence logo using the Frecuency Change Algorithm available in PhosphositePlus® (https://www.phosphosite.org//sequenceLogoAction.action) (Hornbeck et al., 2015).

APPENDIX B. SUPPLEMENTARY FIGURES AND TABLES

POLY(ADP-RIBOSE) POLYMERASE-1 INHIBITION POTENTIATES CELL DEATH AND PHOSPHORYLATION OF DNA DAMAGE RESPONSE PROTEINS IN OXIDATIVE STRESSED RETINAL CELLS

Sandra M. Martín-Guerrero, Pedro Casado, José A. Muñoz-Gámez, María-Carmen Carrasco, Julio Navascués, Miguel A. Cuadros, Juan F. López-Giménez, Pedro R. Cutillas, David Martín-Oliva

Supplementary Fig. 1

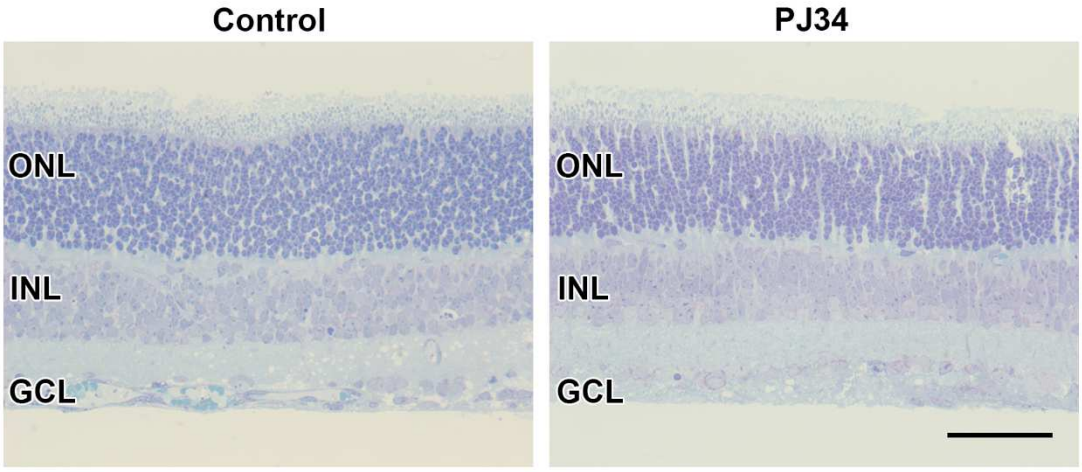

Supplementary Fig. 1. Semithin sections of retinal explants stained with toluidine blue from P12 mice. Control explants (untreated, left panel) and PJ34-treated retinal explants (right panel) showed morphological normal appearances with an organized outer (ONL) and inner (INL) nuclear and ganglion cell (GCL) layers. Scale bar: 50 µm.

Supplementary Fig. 2

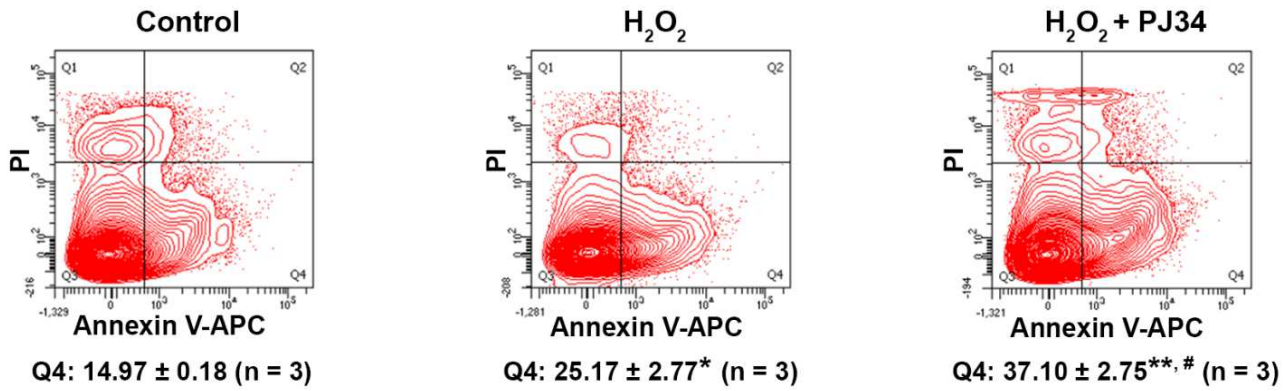

Supplementary Fig. 2. Representative density plots of Annexin V-APC signal (APC-A, x-axis) and propidium iodide (PI) signal (PE-A, y-axis) from retinal explants of P12 mice cultured as we indicated in Fig. 1. Upper left quadrant (Q1) represent necrotic cells (annexin V negative and PI positive cells); upper right (Q2), late apoptotic/secondary necrotic cells (annexin V positive and PI positive cells); lower left quadrant (Q3), alive cells (annexin V negative and PI negative cells); and lower right (Q4), early apoptotic cells (annexin V positive and PI negative cells). The percentage of apoptotic cells (± SEM) in Q4 quadrants for three independent experiments is indicated below the corresponding density plot. *P < 0.05 and **P < 0.01 with respect to control cells and $^{\#}P$ < 0.05 with respect to 3.5 mM H_2O_2.

Supplementary Fig. 3

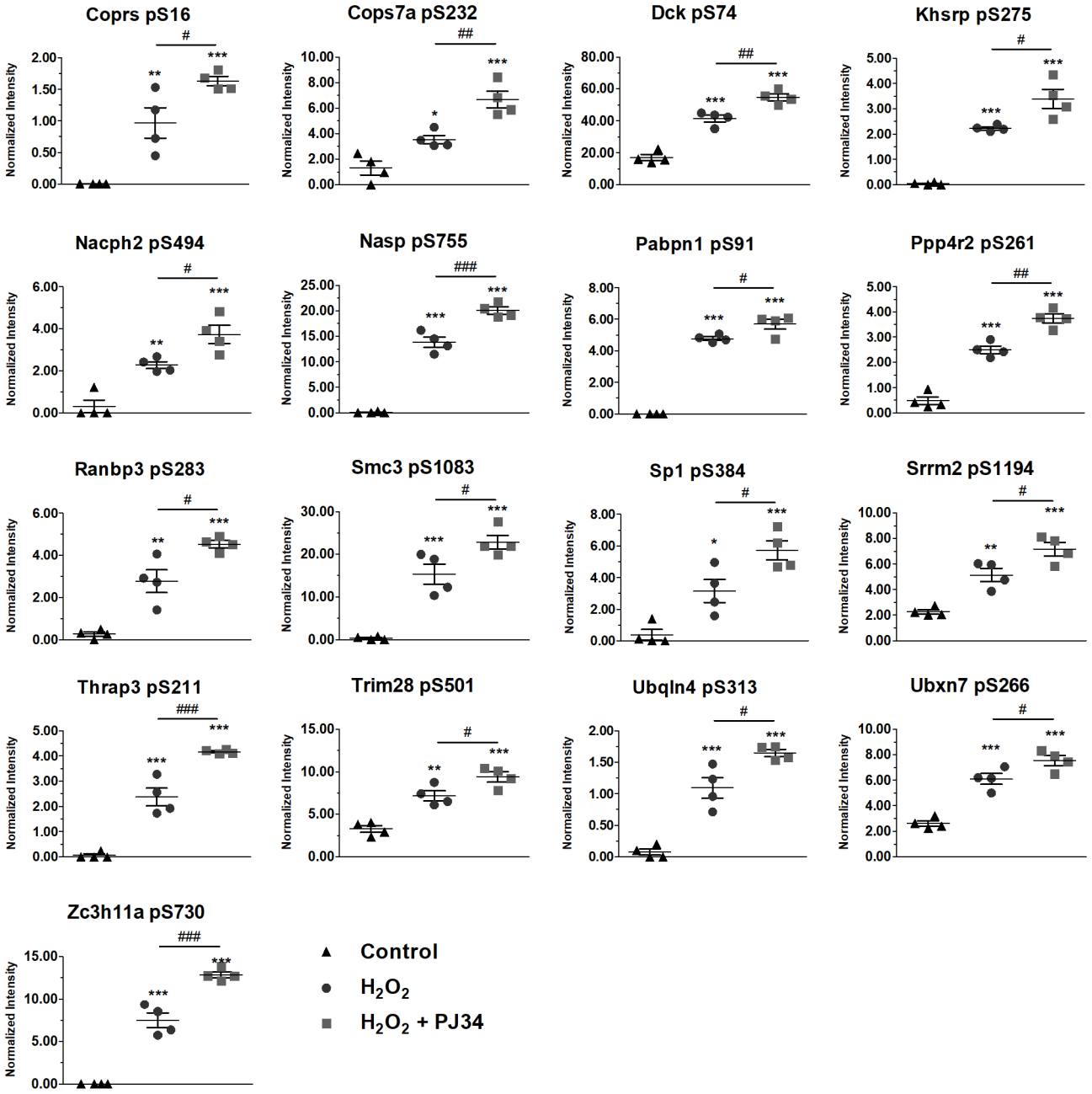

Supplementary Fig. 3. Graphical representation of the signal intensity detected by LC-MS/MS in the differentially expressed common up-regulated phosphopeptides with phosphorylation at SQ motifs in 661W cells. At the y axis is represented the normalized signal intensity obtained by LC-MS/MS analysis for each treatment (represented in the x axis). Control: untreated 661W cells; H_2O_2: H_2O_2-treated cells; H_2O_2 + PJ34: H_2O_2-treated cells in presence of the inhibitor of PARP-1 PJ34. Mean values ± SEM (n = 4) are indicated. *P < 0.05, **P < 0.01 and ***P < 0.001 respect to control; $^{\#}P$ < 0.05, $^{\#\#}P$ < 0.01 and $^{\#\#\#}P$ < 0.001 respect to H_2O_2 treatment.

Supplementary Table 1

Significant unique up-regulated phosphopeptides showing a Fold Change (FC) ≥ 1 after the oxidative treatment in presence of the PARP-1 inhibitor PJ34 (H_2O_2 + PJ34) in 661W cells.

Uniprot ID	Protein name	Gene ID and site PTM	FC
4EBP1	Eukaryotic translation initiation factor 4E-binding protein 1	Eif4ebp1 pT69 pS99 pS100	1.8
AAK1	AP2-associated protein kinase 1	Aak1 pT651	1.4
ABL2	Abelson tyrosine-protein kinase 2	Abl2 pS936	1.0
ABLM1	Actin-binding LIM protein 1	Ablim1 pS466	1.1
ACACA	Acetyl-CoA carboxylase 1	Acaca pS79	1.0
ACTN1	Alpha-actinin-1	Actn1 pS362	1.2
AFAD	Afadin	Mllt4 pS1795	1.3
AFAP1	Actin filament-associated protein 1	Afap1 pS549	1.0
AKA12	A-kinase anchor protein 12	Akap12 pT1191	1.0
ALMS1	Alstrom syndrome protein 1 homolog	Alms1 pS2254	3.3
AMFR	E3 ubiquitin-protein ligase AMFR	Amfr pS542	1.0
AN13A	Ankyrin repeat domain-containing protein 13A	Ankrd13a pS205	1.3
ANO8	Anoctamin-8	Ano8 pS637	1.1
ASPC1	Tether containing UBX domain for GLUT4	Aspscr1 pS279	1.1
ASPP2	Apoptosis-stimulating of p53 protein 2	Tp53bp2 pS328	1.5
ATM	Serine-protein kinase ATM	Atm pS1987	1.2
ATX2L	Ataxin-2-like protein	Atxn2l pS687	1.3
BCAS3	Breast carcinoma-amplified sequence 3 homolog	Bcas3 pS503	1.1
BD1L1	Biorientation of chromosomes in cell division protein 1-like	Bod1l pS2751	1.6
BIRC6	Baculoviral IAP repeat-containing protein 6	Birc6 pS4850	2.9
BIRC6	Baculoviral IAP repeat-containing protein 6	Birc6 pS593	1.1
BOP1	Ribosome biogenesis protein BOP1	Bop1 pT83 pS84	9.1
BOP1	Ribosome biogenesis protein BOP1	Bop1 pS84	1.0
CASC5	Protein CASC5	Casc5 pS794	1.0
CCDC6	Coiled-coil domain-containing protein 6	Ccdc6 pS233 pS237	1.0
CCDC6	Coiled-coil domain-containing protein 6	Ccdc6 pS424 pT427	1.1
CCNE1	G1/S-specific cyclin-E1	Ccne1 pS385	1.0
CD2AP	CD2-associated protein	Cd2ap pT87	1.4
CDC23	Cell division cycle protein 23 homolog	Cdc23 pT562	1.0

CDC27	Cell division cycle protein 27 homolog	Cdc27 pS365	1.3
CDC5L	Cell division cycle 5-like protein	Cdc5l pT385 pT396	1.2
CK084	Uncharacterized protein C11orf84 homolog	pS249 pS252	1.2
CLCA	Calcium-activated chloride channel regulator 1	Clca1 pS223	1.4
CO043	CO043	CO043 pT149	1.1
CP110	Centriolar coiled-coil protein of 110 kDa	Ccp110 pT428	1.2
CPSF6	Cleavage and polyadenylation specificity factor subunit 6	Cpsf6 pT407	1.0
CPSF6	Cleavage and polyadenylation specificity factor subunit 6	Cpsf6 pS410	1.1
CPSF7	Cleavage and polyadenylation specificity factor subunit 7	Cpsf7 pT203	1.1
CREB1	Cyclic AMP-responsive element-binding protein 1	Creb1 pS108 pS111	1.0
DBNL	Drebrin-like protein	Dbnl pS277	1.2
DCAF6	DDB1- and CUL4-associated factor	Dcaf6 pS336	1.4
DPOA2	DNA polymerase alpha subunit B	Pola2 pS126	1.0
DREB	Drebrin	Dbn1 pS272	1.0
DREB	Drebrin	Dbn1 pS387	1.0
EFCB7	EF-hand calcium-binding domain-containing protein 7	Efcab7 pS212	1.0
EH1L1	EH domain-binding protein 1-like protein 1	Ehbp1l1 pS1331	1.2
EHBP1	EH domain-binding protein 1	Ehbp1 pS676	1.3
EIF3B	Eukaryotic translation initiation factor 3 subunit B	Eif3b pS37 pS40	1.1
EPHA2	Ephrin type-A receptor 2	Epha2 pS898	1.3
EPN1	Epsin-1	Epn1 pS434	1.2
ERC6L	DNA excision repair protein ERCC-6-like	Ercc6l pS1001	1.3
ETV3	ETS translocation variant 3	Etv3 pS139	1.5
FIL1L	Filamin A-interacting protein 1-like	Filip1l pS1047	1.3
FLNC	Filamin-C	Flnc pS2234	1.2
FOXO3	Forkhead box protein O3	Foxo3 pS252	1.8
FRS2	Fibroblast growth factor receptor substrate 2	Frs2 pT328	8.7
FXR1	Fragile X mental retardation syndrome-related protein 1	Fxr1 pT398	1.0
G3BP1	Ras GTPase-activating protein-binding protein 1	G3bp1 pT230 pS231	2.2
GAPD1	GTPase-activating protein and VPS9 domain-containing protein 1	Gapvd1 pS746	1.6
GGNB2	Gametogenetin-binding protein 2	Ggnbp2 pS360	1.5
GOGA5	Golgin subfamily A member 5	Golga5 pS155	1.0
GSK3A	Glycogen synthase kinase-3 alpha	Gsk3a pS21	1.1
GTSE1	G2 and S phase-expressed protein 1	Gtse1 pS73	1.1
GTSE1	G2 and S phase-expressed protein 1	Gtse1 pS605	1.4

GTSE1	G2 and S phase-expressed protein 1	Gtse1 pS68	1.2
H13	Histone H1.3	Hist1h1d pS37	1.5
H2AX	Histone H2AX	H2afx pS140	1.0
HDGF	Hepatoma-derived growth factor	Hdgf pT200 pS202	1.6
HECD1	E3 ubiquitin-protein ligase HECTD1	Hectd1 pS1392	1.3
HELZ	Probable helicase with zinc finger domain	Helz pS1788	1.1
HMOX1	Heme oxygenase 1	Hmox1 pS229	1.3
HPBP1	Hsp70-binding protein 1	Hspbp1 pS349	1.0
HTSF1	HIV Tat-specific factor 1 homolog	Htatsf1 pS705	1.1
IF4B	Eukaryotic translation initiation factor 4B	Eif4b pT500 pS504	1.0
IF4G1	Eukaryotic translation initiation factor 4 gamma 1	Eif4g1 pS1211	1.1
JUNB	Transcription factor jun-B	Junb pT252 pS256	1.0
JUNB	Transcription factor jun-B	Junb pT252	1.1
KC1E	Casein kinase I isoform epsilon	Csnk1e pS389	1.0
KIF11	Kinesin-like protein KIF11	Kif11 pS988	1.1
KIF15	Kinesin-like protein KIF15	Kif15 pS1141	1.1
KS6A3	Ribosomal protein S6 kinase alpha-3	Rps6ka3 pS369 pS375	1.6
LAP2	Protein LAP2	Erbb2ip pS1077	1.1
LARP4	La-related protein 4	Larp4 pS69	1.0
LC7L3	Luc7-like protein 3	Luc7l3 pS110	8.3
LIN54	Protein lin-54 homolog	Lin54 pS310	1.2
LIPB1	Liprin-beta-1	Ppfibp1 pS595	2.0
LRC47	Leucine-rich repeat-containing protein 47	Lrrc47 pT521	1.0
MACF1	Microtubule-actin cross-linking factor 1	Macf1 pS5551	1.0
MAP1B	Microtubule-associated protein 1B	Map1b pS1151	1.3
MAP1B	Microtubule-associated protein 1B	Map1b pS1778 pS1781 pT1784	1.0
MAP4	Microtubule-associated protein 4	Map4 pS617	1.1
MAP4	Microtubule-associated protein 4	Map4 pS475	1.0
MAP4	Microtubule-associated protein 4	Map4 pS517	1.0
MAP6	Microtubule-associated protein 6	Map6 pS632	1.9
MARCS	Myristoylated alanine-rich C-kinase substrate	Marcks pS113	9.0
MAST4	Microtubule-associated serine/threonine-protein kinase 4	Mast4 pS2549	1.2
MDC1	Mediator of DNA damage checkpoint protein 1	Mdc1 pT325	1.4
MOES	Moesin	Msn pS576	1.0
MPRIP	Myosin phosphatase Rho-interacting protein	Mprip pS617	1.1

MXRA7	Matrix-remodeling-associated protein 7	Mxra7 pS79 pS96	8.3
MYC	Myc proto-oncogene protein	Myc pS71	1.4
MYPT1	Protein phosphatase 1 regulatory subunit 12A	Ppp1r12a pS299	1.0
NCK5L	Nck-associated protein 5-like	Nckap5l pS473	1.1
NEST	Nestin	Nes pS841	1.1
NFIL3	Nuclear factor interleukin-3-regulated protein	Nfil3 pS353	1.8
NOP2	Probable 28S rRNA (cytosine-C(5))-methyltransferase	Nop2 pS59	1.1
NUP93	Nuclear pore complex protein Nup93	Nup93 pS52	1.3
ODPA	Pyruvate dehydrogenase E1 component subunit alpha, somatic form, mitochondrial	Pdha1 pS232	1.3
OTUB1	Ubiquitin thioesterase OTUB1	Otub1 pS16	1.0
P66B	Transcriptional repressor p66-beta	Gatad2b pS136	1.1
PA24A	Cytosolic phospholipase A2	Pla2g4a pS726	1.3
PAIRB	Plasminogen activator inhibitor 1 RNA-binding protein	Serbp1 pS252	2.3
PAK1	Serine/threonine-protein kinase PAK 1	Pak1 pS204	1.4
PAK2	Serine/threonine-protein kinase PAK 2	Pak2 pS197	1.1
PAXI	Paxillin	Pxn pS83	1.0
PDXD1	Pyridoxal-dependent decarboxylase domain-containing protein 1	Pdxdc1 pT687 pT691	1.3
PHAR4	Phosphatase and actin regulator 4	Phactr4 pT146	1.0
PHF2	Lysine-specific demethylase PHF2	Phf2 pS848	1.1
PNISR	Arginine/serine-rich protein PNISR	Pnisr pS726	1.2
PP1RA	Serine/threonine-protein phosphatase 1 regulatory subunit 10	Ppp1r10 pS313	1.0
PP2BA	Serine/threonine-protein phosphatase 2B catalytic subunit alpha isoform	Ppp3ca pS462	3.8
PPR18	Phostensin	Ppp1r18 pS194	1.0
PRC2C	Protein PRRC2C	Prrc2c pS102	1.7
PRUN2	Protein prune homolog 2	Prune2 pS704	2.0
PSA5	Proteasome subunit alpha type-5	Psma5 pS56	1.1
PTRF	Polymerase I and transcript release factor	Ptrf pS169	1.1
RAI14	Ankycorbin	Rai14 pS318	1.2
RBM34	RNA-binding protein 34	Rbm34 pS20	1.0
RHG17	Rho GTPase-activating protein 17	Arhgap17 pT730 pT734 pT736	1.6
RIPK3	Receptor-interacting serine/threonine-protein kinase 3	Ripk3 pS179	1.2
RLA2	60S acidic ribosomal protein P2	Rplp2 pS74	1.0
RTN4	Reticulon-4	Rtn4 pT430	1.1
SAFB1	Scaffold attachment factor B1	Safb pS354	9.7

SAFB2	Scaffold attachment factor B2	Safb2 pS375	2.8
SF3A1	Splicing factor 3A subunit 1	Sf3a1 pT348 pS357	8.6
SH3G1	Endophilin-A2	Sh3gl1 pS288	1.1
SPG20	Spartin	Spg20 pS126	1.0
SQSTM	Sequestosome-1	Sqstm1 pS368	1.6
SQSTM	Sequestosome-1	Sqstm1 pT272	1.1
SRRM2	Serine/arginine repetitive matrix protein 2	Srrm2 pS1209 pS1216	1.7
SRRM2	Serine/arginine repetitive matrix protein 2	Srrm2 pS2646	1.1
SSA27	Sjoegren syndrome/scleroderma autoantigen 1 homolog	Sssca1 pS78	2.8
SYDE1	Rho GTPase-activating protein SYDE1	Syde1 pS576	2.7
SYNE2	Nesprin-2	Syne2 pS4184	1.1
SYNRG	Synergin gamma	Synrg pS1067	1.0
SYNRG	Synergin gamma	Synrg pS576	1.2
T22D4	TSC22 domain family protein 4	Tsc22d4 pS165	1.2
T22D4	TSC22 domain family protein 4	Tsc22d4 pS271	1.1
TAB2	TGF-beta-activated kinase 1 and MAP3K7-binding protein 2	Tab2 pS584	1.0
TB182	182 kDa tankyrase-1-binding protein	Tnks1bp1 pS1657	1.4
TBC15	TBC1 domain family member 15	Tbc1d15 pS32	1.1
TBC8B	TBC1 domain family member 8B	Tbc1d8b pS358	1.4
TBCD4	TBC1 domain family member 4	Tbc1d4 pS595	1.1
TBCD5	TBC1 domain family member 5	Tbc1d5 pS565 pS568	1.0
TISD	Zinc finger protein 36, C3H1 type-like 2	Zfp36l2 pS464	1.6
TNR6A	Trinucleotide repeat-containing gene 6A protein	Tnrc6a pS1804	1.1
TP53B	Tumor suppressor p53-binding protein 1	Tp53bp1 pS816	1.1
TPC10	Trafficking protein particle complex subunit 10	Trappc10 pS708	1.0
TPC10	Trafficking protein particle complex subunit 10	Trappc10 pS685	1.1
TYY1	Transcriptional repressor protein YY1	Yy1 pS247	1.2
UBE2O	(E3-independent) E2 ubiquitin-conjugating enzyme UBE2O	Ube2o pS394	1.2
UBR4	E3 ubiquitin-protein ligase UBR4	Ubr4 pS362	1.1
WDTC1	WD and tetratricopeptide repeats protein 1	Wdtc1 pS227	1.1
ZBED6	Zinc finger BED domain-containing protein 6	Zbed6 pS809	8.9
ZC3HD	Zinc finger CCCH domain-containing protein 13	Zc3h13 pS1484	1.1
ZCHC8	Zinc finger CCHC domain-containing protein 8	Zcchc8 pS599 pS610	9.4
ZFR	Zinc finger RNA-binding protein	Zfr pS1054	1.0

PTM: Post-translational modification, FC: Fold Change of phosphopeptides in H_2O_2 + PJ34 treatment compared to control.

Supplementary Table 2

Differentially expressed common up-regulated phosphopeptides showing a Fold Change (FC) ≥ 1 in both oxidative treatments (with and without PJ34).

Uniprot ID	Protein name	Gene ID and potential site PTM	PTM motif	Effect of PJ34 in phosphorylation
ATRX	Transcriptional regulator ATRX	Atrx pS111	AATEN**S**ENDIT	Increased
BRCA1*	Breast cancer type 1 susceptibility protein homolog	Brca1 pS1422	NENPV**S**QNLKS	Increased
CLIC4	Chloride intracellular channel protein 4	Clic4 pS167	EIDEN**S**MEDIK	Increased
CNDH2*	Condensin-2 complex subunit H2	Ncaph2 pS494	QETEL**S**QRIRD	Increased
COPRS*	Coordinator of PRMT5 and differentiation stimulator	Coprs pS16	PGERS**S**QEAPS	Increased
CSN7A*	COP9 signalosome complex subunit 7a	Cops7a pS232	AAAAT**S**QDPEQ	Increased
DCK*	Deoxycytidine kinase	Dck pS74	EELTT**S**QKSGG	Increased
EIF3B	Eukaryotic translation initiation factor 3 subunit B	Eif3b pS111	ARGHP**S**AGAEE	Decreased
EIF3B	Eukaryotic translation initiation factor 3 subunit B	Eif3b pS111 pS120 pS123	ARGHP**S**AGAEE EEEGG**S**DGSAA GGSDG**S**AAEAE	Decreased
FLNB	Filamin-B	Flnb pS2487	ANETS**S**ILVES	Increased
FUBP2*	Far upstream element-binding protein 2	Khsrp pS275	LIQDG**S**QNTNV	Increased
GSH1	Glutamate--cysteine ligase catalytic subunit	Gclc pS8	LLSQG**S**PLSWE	Increased
GSK3A	Glycogen synthase kinase-3 alpha	Gsk3a pS21	RARTS**S**FAEPG	Increased
HMGN1	Non-histone chromosomal protein HMG-14	Hmgn1 pS7	PKRKV**S**ADGAA	Decreased
HMOX1	Heme oxygenase 1	Hmox1 pS242	RQRPA**S**LVQDT	Increased
I2BP2	Interferon regulatory factor 2-binding protein 2	Irf2bp2 pS438 pS443	TTRRN**S**SSPPS SSSPP**S**PSSMN	Decreased
KIF23	Kinesin-like protein KIF23	Kif23 pS720	SNSCS**S**ISVAS	Increased
MDC1*	Mediator of DNA damage checkpoint protein 1	Mdc1 pS975	QSLLT**S**QSQKQ	Increased
NASP*	Nuclear autoantigenic sperm protein	Nasp pS755	ENQAE**S**QTAEG	Increased
NEDD4	E3 ubiquitin-protein ligase NEDD4	Nedd4 pS309	TRRQI**S**EDVDG	Decreased
NEST	Nestin	Nes pS840	QESLR**S**LDENQ	Increased
NFIA	Nuclear factor 1 A-type	Nfia pS303 pS310	TKRLK**S**VEDEM EDEMD**S**PGEEP	Decreased
P66B	Transcriptional repressor p66-beta	Gatad2b pT121 pS123 pS130	DRGRL**T**PSPDI GRLTP**S**PDIIV DIIVL**S**DNEAS	Increased
PABP2*	Polyadenylate-binding protein 2	Pabpn1 pS91	SGAPG**S**QEEEE	Increased

PLEC	Plectin	Plec pS2586	IQRQQ**S**DHDAE	Decreased
PP4R2	Serine/threonine-protein phosphatase 4 regulatory subunit 2	Ppp4r2 pS354	EGSGV**S**PAQTD	Increased
PP4R2*	Serine/threonine-protein phosphatase 4 regulatory subunit 2	Ppp4r2 pS261	VRETA**S**QTVSG	Increased
RANB3*	Ran-binding protein 3	Ranbp3pS283	GSESS**S**QEAAP	Increased
SAC2	Phosphatidylinositide phosphatase SAC2	Inpp5f pS829	LWKSD**S**SLETM	Increased
SMC3*	Structural maintenance of chromosomes protein 3	Smc3 pS1083	ERGSG**S**QSSVP	Increased
SP1*	Transcription factor Sp1	Sp1 pS384	GSLQG**S**QQKEG	Increased
SRRM2*	Serine/arginine repetitive matrix protein 2	Srrm2 pS1194	LLPNS**S**QDELM	Increased
SUGP1	SURP and G-patch domain-containing protein 1	Sugp1 pS336	SLRRK**S**APEAL	Increased
SZRD1	SUZ domain-containing protein	Szrd1 pS105 pS107	RRILG**S**ASPEE ILGSA**S**PEEEQ	Decreased
TIF1B*	Transcription intermediary factor 1-beta	Trim28 pS501	DLTSD**S**QPPVF	Increased
TR150*	Thyroid hormone receptor-associated protein 3	Thrap3 pS210	FSGGT**S**QDIKG	Increased
UBQL4*	Ubiquilin-4	Ubqln4 pS313	SDNSS**S**QPLRT	Increased
UBXN7*	UBX domain-containing protein 7	Ubxn7 pS266	DASED**S**QLEAA	Increased
WDR13	WD repeat-containing protein 13	Wdr13 pS116 pY117	SVSRG**S**YQLQA VSRGS**Y**QLQAQ	Decreased
ZC11A*	Zinc finger CCCH domain-containing protein 11A	Zc3h11a pS730	SGPSS**S**QTATK	Increased

PTM: Post-translational modification; *Proteins with phosphorylation at SQ motif.